CHALMERS

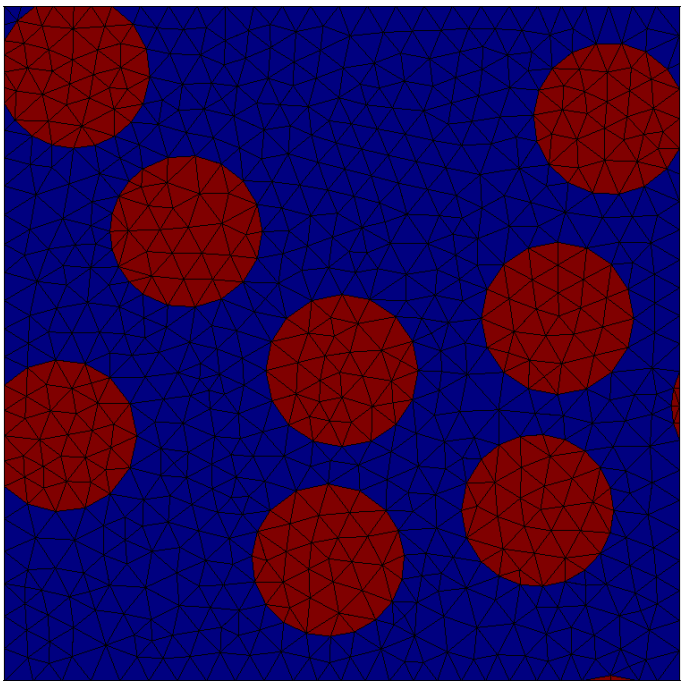

On Homogenization and Virtual Testing of Nonlinear Composites

Master's thesis in Solid and Fluid Mechanics

ROBIN ANDERSSON

Department of Applied Mechanics
Division of Material and Computational Mechanics
CHALMERS UNIVERSITY OF TECHNOLOGY
Göteborg, Sweden 2011
Master's thesis 2011:20

MASTER'S THESIS IN SOLID AND FLUID MECHANICS

On Homogenization and Virtual Testing of Nonlinear Composites

ROBIN ANDERSSON

Department of Applied Mechanics
Division of Material and Computational Mechanics
CHALMERS UNIVERSITY OF TECHNOLOGY
Göteborg, Sweden 2011

On Homogenization and Virtual Testing of Nonlinear Composites
ROBIN ANDERSSON

Master's thesis in Solid and Fluid Mechanics 2011:20
ISSN 1652-8557
Department of Applied Mechanics
Division of Material and Computational Mechanics
Chalmers University of Technology
SE-412 96 Göteborg
Sweden
Telephone: +46 (0)31-772 1000

Cover:
A meshed RVE with circular inclusions.

Chalmers Reproservice
Göteborg, Sweden 2011

On Homogenization and Virtual Testing of Nonlinear Composites
Master's thesis inSolid and Fluid Mechanics
ROBIN ANDERSSON
Department of Applied Mechanics
Division of Material and Computational Mechanics
Chalmers University of Technology

Abstract

The mechanical properties of a macroscopic homogenous material, such as stiffness and yield limit, depend on its physical structure on different subscales. To reveal the subscale mechanical behavior, multiscale modeling and computational homogenization on Representative Volume Elements (RVE) can be adopted.

The main purpose of this work is to establish computable upper and lower bounds of the macroscale strain energy, for nonlinear response, within a given confidence due to statistical sampling. Such bounds have previously been derived in the case of linear elasticity, but are here extended to total deformation plasticity with linear hardening. Numerical examples are given based on "virtual testing" of RVEs with circular inclusions embedded in a matrix material.

Furthermore, a macroscopic constitutive model based on the energy bounds is constructed by fitting constants to the results obtained by the virtual testing procedure. Finally, the calibrated macroscopic model is compared to the "best" RVE, i.e. the most representative realization.

Keywords: Homogenization, RVE, FEM, energy bounds

Preface

The study at hand was made as a master's thesis within the Solid and Fluid Mechanics master program at Chalmers University of Technology during the spring semester of 2011.

I would like to thank my supervisors, Doctor Fredrik Larsson and Professor Kenneth Runesson, for all their help and encouragement. Without their support during the work, this project would have been impossible.

Contents

1 Introduction

1.1 Background

The mechanical properties of a material, such as stiffness and yield limit, depend on its physical structure on different subscales. Since all materials are heterogeneous at some length scale, bridging the properties is an important topic, c.f. Besson et al. [2]. For example, the macroscopic yield limit of a metal might depend on the grain size and orientation while the properties of the grains depend on its phase structure etc.

Determining the behavior of the material on one length scale by information from other length scales is known as multiscale modeling. One of the advantages of multiscale modeling, in contrast to more empirical methods, is that subscale phenomenon can be revealed which leads to a deeper understanding of the mechanisms that determine the material behavior, c.f. Nilenius et al. [9].

The classical approach when constructing a constitutive model is to consider the material at the macroscopic length scale as a homogeneous medium and the subscale heterogeneities are accounted for only implicitly by for example fitting constants to experimental curves. Another, more fundamental, approach is to account for subscale heterogeneities by averaging the influence of their properties to obtain effective properties that holds on the macroscale. This process is called homogenization, c.f. Besson et al. [2], Roters et al. [12], Ostoja-Starzewski [10] and Geers et al. [4]. There exist several closed form analytical homogenization methods, but also computer based schemes. The latter are often refered to as computational homogenization, c.f. Geers et al. [4], Roters et al. [12] Miehe et al. [8], Asada and Ohno [1] and Doghri and Ouaar [3]. In order to perform the computational homogenization, a finite cell that statistically represents the subscale heterogeneities is considered. This cell is called a Representative Volume Elment (RVE). The effective properties of the RVE should converge towards the true values as the size of the RVE is increased.

In practice, Finite Element Analysis (FEA) is often used to solve problems in solid mechanics and can of course also be used when studying multiscale modeling, see for example Quilici and Cailletaud [11]. If for example the beam problem in Figure 1.1.1 should be considered, the classical approach would have been to solve the problem for the unknown displacements, calculate the strain and then put the strains in the Gauss points into a constitutive model in order to obtain the corresponding stresses. If, however, multiscale modeling would have been used, the strain in a Gauss point would have been considered as the macroscale strain for a new FE-problem where a RVE should be considered. The RVE-problem would have been solved for the displacements and in a postprocessing step the stresses should have been homogenized to obtain the effective stress of the RVE, which would then been put back into the macroscale beam problem. Techniques like these are called FE^2, c.f. Geers et al. [4]. Also note that both classical constitutive models and FE^2 might be used in the same macroscale FE-model.

As the computers have become more powerful the last decades, the use of multiscale modeling has grown and nowadays a lot of examples may be found. It is not possible to mention all of

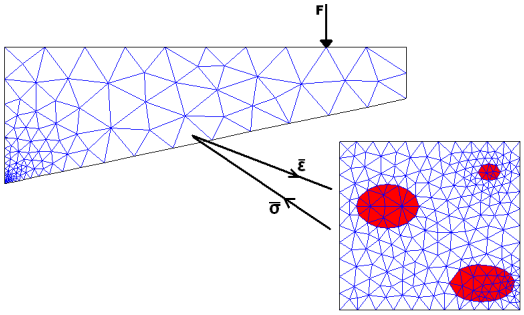

Figure 1.1.1: *A meshed cantilever beam*

them here but two are given below.

An interesting field is the one of corrosion of concrete steel, which is a problem that might decrease the strength of a concrete structure. The steel becomes damaged by a high concentration of chloride ions, which are transported through the porous material by moisture. In order to investigate to what extent the microstructure of the concrete affects the diffusion process, multiscale modeling have been used successfully, see Nilenius et al. [9].

Another example is Wellment et al.[14]. They have suggested a strategy for multiscale modeling and homogenization of granular materials using the Discrete Element Method (DEM). The strategy was then used to fit a elasto-plastic material model.

It is not only in material mechanics multiscale modeling is used. Nilenius et al. [9] mention for example meteorology, particle dynamics and electromagnetism, so the range of disciplines is wide.

1.2 Purpose and scope

The purposes of this study are listed below.

- Develop a strategy for generating a RVE given volume fraction, size and orientation of the particles.
- Establish constitutive models for the components based on plasticity with linear hardening.
- Develop a strategy to compute the full macroscopic energy-strain response with given confidence.
- Develop a strategy to compute the full macroscopic stress-strain response based on the energy curve mentioned above.

Some things might be said about the objectives above. First of all, when it comes to constructing bounds on the macroscopic energy, two intersting works are at hand; Larsson et al. [7], which establishes computable upper bounds for linear elstic materials while approximating the lower bound and Larsson et al. [6], which establishes both upper and lower bounds on the energy for linear elastic materials. It will appear that these papers give a solid foundation

on which upper and lower bounds might be constructed also for materials that are not linear elastic.

Secondly, when it comes to constructing the macroscopic stress-strain response based on the energy bound plots, no obvious foundation have been found. In a lot of studies stress-strain curves have been constructed, but it has been difficult to find any that do it in the sense described above. For example LLorca et al. [5] have constructed stress-strain curves, in the case of elasto-plastic deformation, by averaging the FE-response from a number of RVEs and compared the results with different homogenization methods, but these stress curves have not been based on energy bound plots.

The report is organized in the following manner: The introduction chapter deals with the background of multiscale modeling and homogenization as well as giving some examples of earlier works within the subject. The theoretical background needed to understand the problem is described in the two following chapters. A computational strategy is described in the Virtual Testing chapter and some numerical examples are presented in the Numerical Results chapter. The report is completed with a Conclusion chapter, which also discusses possible future work.

2 Computational homogenization

2.1 Preliminaries

The following sections will discuss some basic topics regarding the general theory of computational homogenization which constitutes the basis for subsequent chapters.

2.1.1 The Representative Volume Element

As been mentioned earlier, most materials are heterogeneous at some length scale. In order to understand different material mechanisms, it is of interest to account for the heterogeneities on the subscales. However, it would be ineffective, not to say practical impossible, to consider the influence of all the individual heterogeneities of a material during for example a stress analysis. Therefore a computational cell of finite size is chosen to represent the material heterogeneities in a statistical way. This kind of cell is called a Representative Volume Element (RVE), since it is considered to be representative for the material at hand. The RVE is often taken as a square in 2D and a cube in 3D and its side length is here denoted $L_\square$, while its volume (or surface in 2D) is denoted $\Omega_\square$.

The RVE is used to calculate *effective properties* via a homogenization of the heterogeneous material. This can be thought of as replacing the heterogeneous material by a homogeneous and the corresponding properties over the RVE are then called the effective properties. If we, for example, are interested in computing the stresses in a material point given the macroscopic strains, we apply the macroscopic strain "load" as well as boundary conditions on the RVE, compute the local strains and stresses and then homogenize them in order to obtain the effective stress corresponding to the macroscopic strain.

An important question is how to choose the RVE in such a way that it really is representative for the material at hand and a lot of literature has been devoted to this subject. c.f. Ostoja-Starzewski [10] and Besson et al. [2]. A more detailed description of how the RVEs were chosen in this study is presented later in section 4.1, but two general issues can be pointed out:

- The size of the RVE should be small enough compared to the macroscale dimensions of the component of interest.

- The size of the RVE should be large enough compared to the subscale heterogeneities in order to obtain a relevant resolution.

What "small enough" and "large enough" really means in practice depends on the problem at hand. If for example a concrete bridge is analyzed it seems reasonable to chose a larger RVE than in the case of a small particle reinforced metal matrix composite, since the heterogeneity dimensions as well as the component dimensions differ considerably.

2.1.2 Governing equations

The mechanical behavior of a solid is often described by partial differential equations (PDE). By considering force equilibrium the following PDE is obtained:

$$-\boldsymbol{P} \cdot \boldsymbol{\nabla} = \boldsymbol{f} \quad \text{in } \Omega_{\square} \tag{2.1.1}$$

where $\boldsymbol{P}$ is the first Piola-Kirchhoff stress tensor, $\boldsymbol{\nabla}$ is the spatial gradient, $\boldsymbol{f}$ are the volume forces and $\Omega_{\square}$ is the domain where the PDE holds. Later it will be assumed that no volume forces exist.

Moreover, it is assumed that the stress can be written as the partial derivative of the strain energy, ψ with respect to the deformation gradient, $\boldsymbol{H}$:

$$\boldsymbol{P}(\boldsymbol{H}) = \frac{\partial \psi(\boldsymbol{H})}{\partial \boldsymbol{H}} \tag{2.1.2}$$

where the deformation gradient is defined in the following way:

$$\boldsymbol{H} \overset{\text{def}}{=} \boldsymbol{u} \otimes \boldsymbol{\nabla} \tag{2.1.3}$$

and $\boldsymbol{u}$ is the displacement.

The displacements might be divided into two parts, namely the macroscopic displacement field, $\boldsymbol{u}^M$ plus a subscale fluctuation, $\boldsymbol{u}^s$:

$$\boldsymbol{u} = \boldsymbol{u}^M + \boldsymbol{u}^s \tag{2.1.4}$$

This relation is illustrated in Figure 2.1.1. An usual assumption, c.f Larsson et al. [7], [6], on the macroscopic displacement is that it vary linear within the RVE in the following way:

$$\boldsymbol{u}^M = \bar{\boldsymbol{u}}(\bar{\boldsymbol{X}}) + \bar{\boldsymbol{H}} \cdot [\boldsymbol{X} - \bar{\boldsymbol{X}}] \text{ for } \boldsymbol{X} \in \Omega_{\square} \tag{2.1.5}$$

where $\bar{\boldsymbol{u}}(\bar{\boldsymbol{X}})$ is a constant macroscopic displacement, $\bar{\boldsymbol{H}}$ is the macroscopic deformation gradient and $\bar{\boldsymbol{X}}$ is the centroid of the RVE. The assumption above is called first order homogenization.

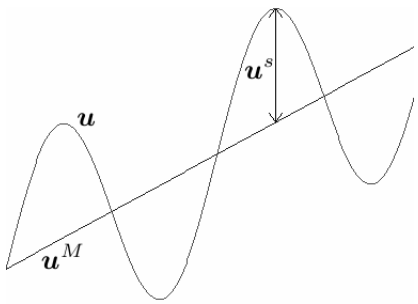

Figure 2.1.1: *The relation between* $\boldsymbol{u}$, $\boldsymbol{u}^M$ and $\boldsymbol{u}^S$.

2.1.3 Boundary conditions

As mentioned briefly earlier, boundary conditions have to be imposed on the RVE. Since the RVE is "cut out" from the component of interest, it is not easy to know what type of boundary condition that is the closest approximation of the real world situation. However, the effective properties are expected to converge towards the true properties as the size of the RVE approaches infinity, regardless choice of boundary conditions on the RVE, see Larsson et al. [6].

Three types of boundary conditions will be considered in this study, namely Dirichlet (essential) where displacements on the boundary are prescribed, Neumann (natural) where tractions on the boundary are prescribed and periodic ones. The periodic boundary conditions are based on a cubic (or quadratic in 2D) RVE where the boundary $\Gamma_\square$ is divided into two parts; the Γ^+ part and Γ^- part, corresponding to the thick and thin boundary in Figure 2.1.2. Every point $\boldsymbol{X}$ on the + part is mirrored onto the − part via a mapping function; $\boldsymbol{X}^- = \boldsymbol{\varphi}(\boldsymbol{X}^+)$.

Two assumptions are made for this kind of boundary condition:

- $\boldsymbol{u}^s(\boldsymbol{X}^+) - \boldsymbol{u}^s(\boldsymbol{X}^-) = \boldsymbol{0}$ Periodic fluctuations on the boundaries.
- $\boldsymbol{t}(\boldsymbol{X}^+) + \boldsymbol{t}(\boldsymbol{X}^-) = \boldsymbol{0}$ Anti-periodic tractions on the boundaries, see Figure 2.1.2.

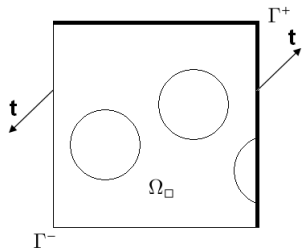

Figure 2.1.2: *A RVE with periodic boundary conditions. The thick boundary corresponds to the* Γ^+ *part, which is the image boundary, while the thin one represents the* Γ^- *boundary which is the mirror boundary. The meaning of anti-periodic tractions is also shown.*

Periodic boundary conditions are exact for materials with a periodic substructure and a good approximation for random substructures, c.f. Larsson et al. [6] and Terada et al. [13]. As will be shown later, the Dirichlet and Neumann conditions might be considered as special cases of the more general periodic boundary conditions.

2.1.4 Effective properties

In this section some effective properties will be studied in detail. Effective properties, such as the deformation gradient, first Piola-Kirchhoff stress and strain energy can be computed as the volume (or area in 2D) average of the RVE:

$$\langle \bullet \rangle_\square \overset{\text{def}}{=} \frac{1}{\mid \Omega_\square \mid} \int_{\Omega_\square} \bullet \, d\Omega \tag{2.1.6}$$

where $\bullet$ is the quantity of interest. So, the effective properties mentioned above might be determined by evaluating the following expressions:

$$\langle \boldsymbol{H} \rangle_{\square}, \langle \boldsymbol{P} \rangle_{\square}, \langle \psi \rangle_{\square} \tag{2.1.7}$$

It is advantageous to study the first two entities in detail. We begin with the volume average of the deformation gradient, $\boldsymbol{H}$:

$$\begin{aligned} \bar{\boldsymbol{H}} \overset{\text{def}}{=} \langle \boldsymbol{H} \rangle_{\square} = \frac{1}{\mid \Omega_{\square} \mid} \int_{\Omega_{\square}} \boldsymbol{H} d\Omega = \frac{1}{\mid \Omega_{\square} \mid} \int_{\Omega_{\square}} \boldsymbol{u} \otimes \boldsymbol{\nabla} d\Omega = \\ = \{\text{Gauss' theorem}\} = \frac{1}{\mid \Omega_{\square} \mid} \int_{\Gamma_{\square}} \boldsymbol{u} \otimes \boldsymbol{N} d\Gamma \end{aligned} \tag{2.1.8}$$

Where $\bar{\boldsymbol{H}}$ is the macroscopic deformation gradient. We continue with the volume average of the first Piola-Kirchhoff stress, $\boldsymbol{P}$.

$$\begin{aligned} \bar{\boldsymbol{P}} \overset{\text{def}}{=} \langle \boldsymbol{P} \rangle_{\square} = \frac{1}{\mid \Omega_{\square} \mid} \int_{\Omega_{\square}} \boldsymbol{P} d\Omega = \frac{1}{\mid \Omega_{\square} \mid} \int_{\Omega_{\square}} \boldsymbol{P} \cdot \boldsymbol{I} d\Omega = \frac{1}{\mid \Omega_{\square} \mid} \int_{\Omega_{\square}} \boldsymbol{P} \cdot \boldsymbol{\nabla} \otimes [\boldsymbol{X} - \bar{\boldsymbol{X}}] d\Omega = \\ = \frac{1}{\mid \Omega_{\square} \mid} \int_{\Omega_{\square}} (\boldsymbol{\nabla} \cdot [\boldsymbol{P}^T \otimes [\boldsymbol{X} - \bar{\boldsymbol{X}}]] - [\boldsymbol{P} \cdot \boldsymbol{\nabla}] \otimes [\boldsymbol{X} - \bar{\boldsymbol{X}}]) d\Omega = \{\text{Gauss' theorem}\} = \\ = \frac{1}{\mid \Omega_{\square} \mid} \int_{\Gamma_{\square}} \boldsymbol{t} \otimes [\boldsymbol{X} - \bar{\boldsymbol{X}}] d\Gamma + \frac{1}{\mid \Omega_{\square} \mid} \int_{\Omega_{\square}} \boldsymbol{f} \otimes [\boldsymbol{X} - \bar{\boldsymbol{X}}] d\Omega \end{aligned} \tag{2.1.9}$$

Where $\bar{\boldsymbol{P}}$ is the macroscopic stress tensor and it was used that $\boldsymbol{t} \overset{\text{def}}{=} \boldsymbol{N} \cdot \boldsymbol{P}^T$. In the special case of no volume load the equation above reduces to the following:

$$\bar{\boldsymbol{P}} \overset{\text{def}}{=} \langle \boldsymbol{P} \rangle_{\square} = \frac{1}{\mid \Omega_{\square} \mid} \int_{\Gamma_{\square}} \boldsymbol{t} \otimes [\boldsymbol{X} - \bar{\boldsymbol{X}}] d\Gamma \tag{2.1.10}$$

2.1.5 The Hill-Mandel condition

An important topic when it comes to homogenization is the so-called Hill-Mandel condition. It states that the virtual work on the subscale must equal the virtual work on the macroscale:

$$\langle \boldsymbol{P} : \boldsymbol{H} \rangle_{\square} = \langle \boldsymbol{P} \rangle_{\square} : \langle \boldsymbol{H} \rangle_{\square} = \bar{\boldsymbol{P}} : \bar{\boldsymbol{H}} \tag{2.1.11}$$

In order to check if the condition is fulfilled it might be useful to rewrite the left hand term in the equation above in the following way:

$$\langle \boldsymbol{P} : \boldsymbol{H} \rangle_{\square} = \frac{1}{\mid \Omega_{\square} \mid} \int_{\Omega_{\square}} \boldsymbol{P} : \boldsymbol{H} d\Omega = \frac{1}{\mid \Omega_{\square} \mid} \left[\int_{\Omega_{\square}} \boldsymbol{f} \cdot \boldsymbol{u} d\Omega + \int_{\Gamma_{\square}} \boldsymbol{t} \cdot \boldsymbol{u} d\Gamma \right] \tag{2.1.12}$$

where Gauss' theorem was used. If there are no volume loads, this reduces to:

$$\langle \boldsymbol{P} : \boldsymbol{H} \rangle_{\square} = \frac{1}{\mid \Omega_{\square} \mid} \int_{\Gamma_{\square}} \boldsymbol{t} \cdot \boldsymbol{u} d\Gamma \tag{2.1.13}$$

2.2 Canonical form of the RVE-problem

In the following section a canonical form of the RVE-problem will be presented. It is based on the variational formulation presented in Larsson et al. [7] and [6]. Let us consider a RVE occupying the volume $\Omega_\square$. If no volume forces exist, force equilibrium yields:

$$-\boldsymbol{P}\cdot\boldsymbol{\nabla}=\boldsymbol{0}\quad\text{in }\Omega_\square \tag{2.2.1}$$

Furthermore we assume periodic boundary conditions. As mentioned before, this demands anti-periodic tractions along the boundaries. We also have a kinematic condition that relate the displacements to the macroscale deformation gradient. This gives two equations:

$$\boldsymbol{t}(\boldsymbol{X}^+)+\boldsymbol{t}(\boldsymbol{X}^-)=\boldsymbol{0} \tag{2.2.2}$$

$$\boldsymbol{u}(\boldsymbol{X}^+)-\boldsymbol{u}(\boldsymbol{X}^-)=\bar{\boldsymbol{H}}\cdot[\boldsymbol{X}^+-\boldsymbol{X}^-] \tag{2.2.3}$$

If equation 2.2.1 is rewritten in weak form and scaled by $\frac{1}{|\Omega_\square|}$, it yields:

$$a_\square(\boldsymbol{u};\delta\boldsymbol{u})-\frac{1}{|\,\Omega_\square\,|}\int_{\Gamma_\square}\boldsymbol{t}\cdot\delta\boldsymbol{u}d\Gamma=0 \tag{2.2.4}$$

where

$$a_\square(\boldsymbol{u};\delta\boldsymbol{u})\overset{\text{def}}{=}\frac{1}{|\,\Omega_\square\,|}\int_{\Omega_\square}\boldsymbol{P}:[\delta\boldsymbol{u}\otimes\boldsymbol{\nabla}]d\Omega \tag{2.2.5}$$

Before continuing the derivations, a new denotation will be introduced, namely the "jump", which is defined as follows:

$$[\![\bullet]\!]\overset{\text{def}}{=}\bullet(\boldsymbol{X}^+)-\bullet(\boldsymbol{X}^-)=\bullet(\boldsymbol{X}^+)-\bullet(\boldsymbol{\varphi}(\boldsymbol{X}^+))\quad\text{on }\Gamma_\square^+ \tag{2.2.6}$$

The second term in equation (2.2.4) might now be rewritten in the following way:

$$\begin{aligned}\frac{1}{|\,\Omega_\square\,|}\int_{\Gamma_\square}\boldsymbol{t}\cdot\delta\boldsymbol{u}d\Gamma=\frac{1}{|\,\Omega_\square\,|}\int_{\Gamma_\square^+}\boldsymbol{t}(\boldsymbol{X}^+)\cdot\delta\boldsymbol{u}^+d\Gamma+\frac{1}{|\,\Omega_\square\,|}\int_{\Gamma_\square^-}\boldsymbol{t}(\boldsymbol{X}^-)\cdot\delta\boldsymbol{u}^-d\Gamma=\\ \frac{1}{|\,\Omega_\square\,|}\int_{\Gamma_\square^+}\boldsymbol{t}\cdot(\delta\boldsymbol{u}^+-\delta\boldsymbol{u}^-)d\Gamma=\frac{1}{|\,\Omega_\square\,|}\int_{\Gamma_\square^+}\boldsymbol{t}\cdot[\![\delta\boldsymbol{u}]\!]d\Gamma\end{aligned} \tag{2.2.7}$$

Equation (2.2.4) combined with (2.2.7) yields:

$$a_\square(\boldsymbol{u};\delta\boldsymbol{u})-d_\square(\boldsymbol{t},\delta\boldsymbol{u})=0\quad\forall\delta\boldsymbol{u}\in\mathbb{U}_\square \tag{2.2.8}$$

where

$$d_\square(\boldsymbol{t},\delta\boldsymbol{u})\overset{\text{def}}{=}\frac{1}{|\,\Omega_\square\,|}\int_{\Gamma_\square^+}\boldsymbol{t}\cdot[\![\delta\boldsymbol{u}]\!]d\Gamma \tag{2.2.9}$$

and the function space

$$\mathbb{U}_\square=\{\boldsymbol{u}\text{ sufficiently regular in }\Omega_\square,\ \boldsymbol{u}(\boldsymbol{X}_0)=\boldsymbol{0}\} \tag{2.2.10}$$

where the second condition of the function space is needed to prevent rigid body translation.

Equation (2.2.3) can also be written on weak form, but instead of a variation of the displacements a variation of the tractions is considered. Note that the boundary integrals below are due to the fact that the displacements at hand live on the boundaries only.

$$\begin{aligned}\frac{1}{\mid \Omega_\square \mid}\int_{\Gamma_\square^+}[\![\boldsymbol{u}]\!]\cdot\delta\boldsymbol{t}d\Gamma = \frac{1}{\mid \Omega_\square \mid}\int_{\Gamma_\square^+}\delta\boldsymbol{t}\cdot\bar{\boldsymbol{H}}\cdot[\![\boldsymbol{X}]\!]d\Gamma \\ = \{\bar{\boldsymbol{H}}\cdot[\![\boldsymbol{X}]\!] = \bar{\boldsymbol{H}}\cdot[\![\boldsymbol{X}-\bar{\boldsymbol{X}}]\!] = [\![\bar{\boldsymbol{H}}\cdot[\boldsymbol{X}-\bar{\boldsymbol{X}}]]\!]\} = \\ = \frac{1}{\mid \Omega_\square \mid}\int_{\Gamma_\square^+}\delta\boldsymbol{t}\cdot[\![\bar{\boldsymbol{H}}\cdot[\boldsymbol{X}-\bar{\boldsymbol{X}}]]\!]d\Gamma \end{aligned} \tag{2.2.11}$$

where $\bar{\boldsymbol{X}} = \langle\boldsymbol{X}\rangle_\square$. Equation (2.2.11) can be written in a shorter format:

$$d_\square(\delta\boldsymbol{t},\boldsymbol{u}) = d_\square(\delta\boldsymbol{t},\bar{\boldsymbol{H}}\cdot[\boldsymbol{X}-\bar{\boldsymbol{X}}]) \quad \forall\delta\boldsymbol{t}\in\mathbb{T}_\square \tag{2.2.12}$$

which is the weak form of equation (2.2.3). The function space is defined as follows:

$$\mathbb{T}_\square = \{\boldsymbol{t} \text{ sufficiently regular on } \Gamma_\square\} \tag{2.2.13}$$

One more derivation is needed in order to complete the equation system needed to solve a problem with general periodic boundary conditions. Consider the expression for $\bar{\boldsymbol{P}}$ in the case of no volume load from equation (2.1.10) and multiply it with a test function $\delta\bar{\boldsymbol{H}}$. This yields:

$$\begin{aligned}\langle\boldsymbol{P}\rangle_\square : \delta\bar{\boldsymbol{H}} = \bar{\boldsymbol{P}} : \delta\bar{\boldsymbol{H}} = \frac{1}{\mid \Omega_\square \mid}\int_{\Gamma_\square}\boldsymbol{t}\otimes[\boldsymbol{X}-\bar{\boldsymbol{X}}]d\Gamma : \delta\bar{\boldsymbol{H}} = \frac{1}{\mid \Omega_\square \mid}\int_{\Gamma_\square}\boldsymbol{t}\cdot[\delta\bar{\boldsymbol{H}}\cdot[\boldsymbol{X}-\bar{\boldsymbol{X}}]]d\Gamma = \\ \frac{1}{\mid \Omega_\square \mid}\int_{\Gamma_\square^+}\boldsymbol{t}(\boldsymbol{X}^+)\cdot[\delta\bar{\boldsymbol{H}}\cdot[\boldsymbol{X}^+-\bar{\boldsymbol{X}}]]d\Gamma + \frac{1}{\mid \Omega_\square \mid}\int_{\Gamma_\square^-}\boldsymbol{t}(\boldsymbol{X}^-)\cdot[\delta\bar{\boldsymbol{H}}\cdot[\boldsymbol{X}^--\bar{\boldsymbol{X}}]]d\Gamma = \\ \frac{1}{\mid \Omega_\square \mid}\int_{\Gamma_\square^+}\boldsymbol{t}\cdot[\![\delta\bar{\boldsymbol{H}}\cdot[\boldsymbol{X}-\bar{\boldsymbol{X}}]]\!]d\Gamma = d_\square(\boldsymbol{t},\delta\bar{\boldsymbol{H}}\cdot[\boldsymbol{X}-\bar{\boldsymbol{X}}]) \quad \forall\delta\bar{\boldsymbol{H}}\in\mathbb{R}^{(3x3)}\end{aligned} \tag{2.2.14}$$

So, to summarize, the RVE-problem with general periodic boundary conditions results in the following equation system:

$$\begin{aligned}a_\square(\boldsymbol{u};\delta\boldsymbol{u}) - d_\square(\boldsymbol{t},\delta\boldsymbol{u}) = 0 \quad \forall\delta\boldsymbol{u}\in\mathbb{U}_\square \\ d_\square(\delta\boldsymbol{t},\boldsymbol{u}) = d_\square(\delta\boldsymbol{t},\bar{\boldsymbol{H}}\cdot[\boldsymbol{X}-\bar{\boldsymbol{X}}]) \quad \forall\delta\boldsymbol{t}\in\mathbb{T}_\square \\ d_\square(\boldsymbol{t},\delta\bar{\boldsymbol{H}}\cdot[\boldsymbol{X}-\bar{\boldsymbol{X}}]) = \bar{\boldsymbol{P}}:\delta\bar{\boldsymbol{H}} \quad \forall\delta\bar{\boldsymbol{H}}\in\mathbb{R}^{(3x3)}\end{aligned} \tag{2.2.15}$$

It is possible to obtain Dirichlet and Neumann boundary conditions for both strain and stress control by restricting the function spaces $\mathbb{U}_\square$ and $\mathbb{T}_\square$, which is also the subject of the following sections.

2.2.1 Dirichlet boundary conditions with strain control

The following section will consider the weak form of the RVE-problem with Dirichlet boundary conditions and strain control. Strain control means that the macroscopic deformation gradient, $\bar{\boldsymbol{H}}$, is prescribed and the problem is solved for the macroscopic stress $\bar{\boldsymbol{P}}$.

We start with equation (2.2.15) from section 2.2. However, this time $\mathbb{U}_\square$ is restricted according to the Dirichlet boundary conditions:

$$\mathbb{U}_\square^D = \{\boldsymbol{u} \text{ sufficiently regular in } \Omega_\square, \boldsymbol{u} = \hat{\boldsymbol{H}} \cdot [\boldsymbol{X} - \bar{\boldsymbol{X}}] \text{ on } \Gamma_\square, \hat{\boldsymbol{H}} \in \mathbb{R}^{3x3}\} \subset \mathbb{U}_\square \tag{2.2.16}$$

We begin the derivation by considering $(2.2.15)_2$. Since the equation refers to boundary integrals, it might be written in the following way:

$$d_\square(\delta \boldsymbol{t}, \hat{\boldsymbol{H}} \cdot [\boldsymbol{X} - \bar{\boldsymbol{X}}]) = d_\square(\delta \boldsymbol{t}, \bar{\boldsymbol{H}} \cdot [\boldsymbol{X} - \bar{\boldsymbol{X}}]) \tag{2.2.17}$$

This can be expressed explicitly as:

$$[\hat{\boldsymbol{H}} - \bar{\boldsymbol{H}}] : \frac{1}{\mid \Omega_\square \mid} \int_{\Gamma_\square^+} \delta \boldsymbol{t} \otimes [\![\boldsymbol{X} - \bar{\boldsymbol{X}}]\!] d\Gamma = 0 \tag{2.2.18}$$

which gives that $\hat{\boldsymbol{H}} = \bar{\boldsymbol{H}}$.

If equation $(2.2.15)_3$ is developed it will state that $\bar{\boldsymbol{P}} = \langle \boldsymbol{P} \rangle_\square$ which is used in the post-processing. Now, only equation $(2.2.15)_1$ remains. Because of the Dirichlet conditions the testfunctions are required to be zero at the boundaries. Therefore the RVE-problem might be formulated as: Find $\boldsymbol{u} \in \mathbb{U}_\square^D(\bar{\boldsymbol{H}})$ such that

$$a_\square(\boldsymbol{u}; \delta \boldsymbol{u}) = 0 \; \forall \delta \boldsymbol{u} \in \mathbb{U}_\square^D(\boldsymbol{0}) \tag{2.2.19}$$

In order to investigate whether the Dirichlet boundary conditions fulfill the Hill-Mandel relation equation (2.1.13) is used:

$$\begin{aligned} \langle \boldsymbol{P} : \boldsymbol{H} \rangle_\square = \frac{1}{\mid \Omega_\square \mid} \int_{\Gamma_\square} \boldsymbol{t} \cdot \boldsymbol{u} d\Gamma = \frac{1}{\mid \Omega_\square \mid} \int_{\Gamma_\square} \boldsymbol{t} \cdot \bar{\boldsymbol{H}} \cdot [\boldsymbol{X} - \bar{\boldsymbol{X}}] d\Gamma = \\ = \frac{1}{\mid \Omega_\square \mid} \int_{\Gamma_\square} \boldsymbol{N} \cdot \boldsymbol{P}^T \otimes [\boldsymbol{X} - \bar{\boldsymbol{X}}] d\Gamma : \bar{\boldsymbol{H}} = \frac{1}{\mid \Omega_\square \mid} \int_{\Omega_\square} \boldsymbol{P} d\Omega : \bar{\boldsymbol{H}} = \bar{\boldsymbol{P}} : \bar{\boldsymbol{H}} \end{aligned} \tag{2.2.20}$$

So, the Hill-Mandel condition is fulfilled for Dirichlet boundary conditions.

2.2.2 Neumann boundary conditions with strain control

The following section will consider the weak form of the RVE-problem with Neumann boundary conditions and strain control. As in the previous section, we start with equation (2.2.15) from section 2.2. This time $\mathbb{T}_\square$ is restricted according to the Neumann boundary conditions:

$$\mathbb{T}_\square^N = \{\boldsymbol{t} = \hat{\boldsymbol{P}} \cdot \boldsymbol{N} \text{ on } \Gamma_\square, \hat{\boldsymbol{P}} \in \mathbb{R}^{(3x3)}\} \subset \mathbb{T}_\square \tag{2.2.21}$$

It will appear that the following derivation is useful:

$$\begin{aligned} d_\square(\hat{\boldsymbol{P}} \cdot \boldsymbol{N}, \boldsymbol{u}) = \frac{1}{\mid \Omega_\square \mid} \int_{\Gamma_\square^+} (\hat{\boldsymbol{P}} \cdot \boldsymbol{N}) \cdot [\![\boldsymbol{u}]\!] d\Gamma = \hat{\boldsymbol{P}} : \frac{1}{\mid \Omega_\square \mid} \int_{\Gamma_\square^+} [\![\boldsymbol{u}]\!] \otimes \boldsymbol{N} d\Gamma = \\ = \hat{\boldsymbol{P}} : (\frac{1}{\mid \Omega_\square \mid} \int_{\Gamma_\square^+} \boldsymbol{u} \otimes \boldsymbol{N} d\Gamma + \frac{1}{\mid \Omega_\square \mid} \int_{\Gamma_\square^-} \boldsymbol{u} \otimes \boldsymbol{N} d\Gamma) = \hat{\boldsymbol{P}} : \frac{1}{\mid \Omega_\square \mid} \int_{\Gamma_\square} \boldsymbol{u} \otimes \boldsymbol{N} d\Gamma = \\ = \{\text{Gauss' theorem}\} = \hat{\boldsymbol{P}} : \frac{1}{\mid \Omega_\square \mid} \int_{\Omega_\square} \boldsymbol{u} \otimes \boldsymbol{\nabla} d\Omega = \hat{\boldsymbol{P}} : \langle \boldsymbol{H}[\boldsymbol{u}] \rangle_\square \end{aligned} \tag{2.2.22}$$

Furthermore, it should be noted that the following equality, which can also be derived from equation $(2.2.15)_3$, holds:

$$\bar{\boldsymbol{P}} = \frac{1}{\mid \Omega_\square \mid} \int_{\Gamma_\square} \boldsymbol{t} \otimes [\boldsymbol{X} - \bar{\boldsymbol{X}}] d\Gamma = \hat{\boldsymbol{P}} \cdot \frac{1}{\mid \Omega_\square \mid} \int_{\Gamma_\square} \boldsymbol{N} \otimes [\boldsymbol{X} - \bar{\boldsymbol{X}}] d\Gamma =$$
$$\{\text{Gauss' theorem}\} = \hat{\boldsymbol{P}} \cdot \frac{1}{\mid \Omega_\square \mid} \int_{\Omega_\square} \boldsymbol{\nabla} \otimes [\boldsymbol{X} - \bar{\boldsymbol{X}}] d\Omega = \hat{\boldsymbol{P}} \tag{2.2.23}$$

So, with use of the equation above plus $(2.2.15)_1$ and $(2.2.15)_2$ it can be concluded that the RVE-problem might be formulated as: Find $\boldsymbol{u} \in \mathbb{U}_\square$, $\bar{\boldsymbol{P}} \in \mathbb{R}^{3x3}$ such that

$$a_\square(\boldsymbol{u}; \delta\boldsymbol{u}) - \bar{\boldsymbol{P}} : \langle \boldsymbol{H}[\delta\boldsymbol{u}] \rangle_\square = 0 \quad \forall \delta\boldsymbol{u} \in \mathbb{U}_\square \tag{2.2.24}$$
$$\delta\bar{\boldsymbol{P}} : \langle \boldsymbol{H}[\boldsymbol{u}] \rangle_\square = \delta\bar{\boldsymbol{P}} : \bar{\boldsymbol{H}} \quad \forall \delta\bar{\boldsymbol{P}} \in \mathbb{R}^{3x3} \tag{2.2.25}$$

In order to investigate whether the Neumann boundary conditions fulfill the Hill-Mandel relation equation (2.1.13) is used:

$$\langle \boldsymbol{P} : \boldsymbol{H} \rangle_\square = \frac{1}{\mid \Omega_\square \mid} \int_{\Gamma_\square} \boldsymbol{t} \cdot \boldsymbol{u} d\Gamma = \frac{1}{\mid \Omega_\square \mid} \int_{\Gamma_\square} \bar{\boldsymbol{P}} \cdot \boldsymbol{N} \cdot \boldsymbol{u} d\Gamma =$$
$$\frac{1}{\mid \Omega_\square \mid} \bar{\boldsymbol{P}} : \int_{\Gamma_\square} \boldsymbol{u} \otimes \boldsymbol{N} d\Gamma = \frac{1}{\mid \Omega_\square \mid} \bar{\boldsymbol{P}} : \int_{\Omega_\square} \boldsymbol{u} \otimes \boldsymbol{\nabla} d\Omega = \bar{\boldsymbol{P}} : \bar{\boldsymbol{H}} \tag{2.2.26}$$

So, the Hill-Mandel condition is fulfilled for Neumann boundary conditions.

2.2.3 Dirichlet boundary conditions with stress control

The following section will consider Dirichlet boundary condition with stress control, which means that the macroscopic stress, $\bar{\boldsymbol{P}}$, is prescribed and the problem is solved for the macroscopic strain, $\bar{\boldsymbol{H}}$, in the case of a prescribed displacement on the boundaries. As before we begin with equation (2.2.15) and restrict $\mathbb{U}_\square$ to $\mathbb{U}_\square^D$.

Exactly like in the case of Dirichlet boundary condition and strain control, equation $(2.2.15)_2$ imply that $\hat{\boldsymbol{H}} = \bar{\boldsymbol{H}}$.

If it once again is required that the testfunctions should be zero on the boundaries, equation $(2.2.15)_1$ will lose its second term. Moreover, equation $(2.2.15)_3$ can be expressed in the same format as in equation (2.2.14). This yields that the RVE-problem can be stated: Find $\boldsymbol{u} \in \mathbb{U}_\square^D$ such that

$$a_\square(\boldsymbol{u}; \delta\boldsymbol{u}) = 0 \quad \forall \delta\boldsymbol{u} \in \mathbb{U}_\square^D(\boldsymbol{0})$$
$$\langle \boldsymbol{P} \rangle_\square : \delta\bar{\boldsymbol{H}} = \bar{\boldsymbol{P}} : \delta\bar{\boldsymbol{H}} \quad \forall \delta\bar{\boldsymbol{H}} \in \mathbb{R}^{3x3} \tag{2.2.27}$$

2.2.4 Neumann boundary conditions with stress control

The following section will consider the weak form of the RVE-problem with Neumann boundary conditions and stress control. This means that the macroscopic stress, $\bar{\boldsymbol{P}}$, is prescribed and the problem is solved for the macroscopic strain $\bar{\boldsymbol{H}}$.

With help of equation (2.2.22) the second term of equation $(2.2.15)_1$ can be written as $\hat{\boldsymbol{P}} : \langle \boldsymbol{H}[\delta \boldsymbol{u}] \rangle_\square$. Moreover, equation $(2.2.15)_3$ imply that $\hat{\boldsymbol{P}} = \bar{\boldsymbol{P}}$. So the problem might be formulated as: Find $\boldsymbol{u} \in \mathbb{U}_\square$ such that

$$a_\square(\boldsymbol{u}; \delta \boldsymbol{u}) = \bar{\boldsymbol{P}} : \langle \boldsymbol{H}[\delta \boldsymbol{u}] \rangle_\square \quad \forall \delta \boldsymbol{u} \in \mathbb{U}_\square \tag{2.2.28}$$

With help of equation (2.2.22) it can also be understood that equation $(2.2.15)_2$ imply that $\bar{\boldsymbol{H}} = \langle \boldsymbol{H}[\boldsymbol{u}] \rangle_\square$, which is used in the postprocessing.

3 Energy bounds

In the following sections different statistical bounds on the energy of the RVE-problem will be discussed. The aim is to establish computable upper and lower bounds on the strain energy.

3.1 Strain energy

The potential energy of the RVE-problem with macroscale strain control can be postulated as follows:

$$\Pi_\square(\boldsymbol{u},\boldsymbol{t}) \stackrel{\text{def}}{=} \frac{1}{\mid \Omega_\square \mid}\int_{\Omega_\square}\psi(\boldsymbol{H}[\boldsymbol{u}])d\Omega - \frac{1}{\mid \Omega_\square \mid}\int_{\Gamma_\square^+}[\![\boldsymbol{u}-\bar{\boldsymbol{H}}\cdot[\boldsymbol{X}-\bar{\boldsymbol{X}}]]\!]\cdot\boldsymbol{t}d\Gamma = \\ \langle\psi\rangle_\square - d_\square(\boldsymbol{t},\boldsymbol{u}) + d_\square(\boldsymbol{t},\bar{\boldsymbol{H}}\cdot[\boldsymbol{X}-\bar{\boldsymbol{X}}]) \tag{3.1.1}$$

Stationarity of the potential in the function space $\mathbb{U}_\square \times \mathbb{T}_\square$ requires that the partial derivatives with respect to $\boldsymbol{u}$ and $\boldsymbol{t}$ vanish:

$$\Pi'_{\square,u}(\boldsymbol{u},\boldsymbol{t};\delta\boldsymbol{u}) = 0 \quad \forall\delta\boldsymbol{u}\in\mathbb{U}_\square \tag{3.1.2}$$

$$\Pi'_{\square,t}(\boldsymbol{u},\boldsymbol{t};\delta\boldsymbol{t}) = 0 \quad \forall\delta\boldsymbol{t}\in\mathbb{T}_\square \tag{3.1.3}$$

which give the following two relations:

$$a_\square(\boldsymbol{u};\delta\boldsymbol{u}) - d_\square(\boldsymbol{t},\delta\boldsymbol{u}) = 0 \quad \forall\delta\boldsymbol{u}\in\mathbb{U}_\square \tag{3.1.4}$$

$$d_\square(\delta\boldsymbol{t},\boldsymbol{u}) = d_\square(\delta\boldsymbol{t},\bar{\boldsymbol{H}}\cdot[\boldsymbol{X}-\bar{\boldsymbol{X}}]) \quad \forall\delta\boldsymbol{t}\in\mathbb{T}_\square \tag{3.1.5}$$

where equation (2.1.2) was used in the first relation. The two equations above are identical to equation $(2.2.15)_1$-$(2.2.15)_2$ (periodic boundary conditions with strain control), so the choice of potential energy is correct.

If the functions that fulfill the equations are found, the two latter terms of equation (3.1.1) will vanish and the remaining one is the definition of the macroscopic strain energy, since $\bar{\psi}_\square\{\bar{\boldsymbol{H}}\} = \langle\psi\rangle_\square = \frac{1}{|\Omega_\square|}\int_{\Omega_\square}\psi(\boldsymbol{H}[\boldsymbol{u}])d\Omega$. This means that the macroscopic strain energy can be obtained by a min max function in the following way:

$$\bar{\psi}_\square\{\bar{\boldsymbol{H}}\} = \min_{\hat{\boldsymbol{u}}\in\mathbb{U}_\square}\max_{\hat{\boldsymbol{t}}\in\mathbb{T}_\square}\Pi_\square(\bar{\boldsymbol{H}};\hat{\boldsymbol{u}},\hat{\boldsymbol{t}}) \tag{3.1.6}$$

This requires that the second derivative with respect to the displacements is positive:

$$\Pi''_{uu}(\boldsymbol{u},\boldsymbol{t};\delta\boldsymbol{u},\delta\boldsymbol{u}) = a'_\square(\boldsymbol{u};\delta\boldsymbol{u},\delta\boldsymbol{u}) = \frac{1}{\mid \Omega_\square \mid}\int_{\Omega_\square}[\delta\boldsymbol{u}\otimes\boldsymbol{\nabla}]:\mathsf{L}:[\delta\boldsymbol{u}\otimes\boldsymbol{\nabla}]d\Omega > 0 \tag{3.1.7}$$

where L is the tangential stiffness.

The great advantage of writing the strain energy on the form of equation (3.1.6) is that in order to obtain the strain energy for Dirichlet and Neumann boundary conditions, $\mathbb{U}_\square$ and $\mathbb{T}_\square$ are simply restricted.

3.2 Stress energy

In the case of macroscale stress control, it is possible to define the stress energy in the following manner:

$$\bar{\psi}^*_\square\{\bar{\boldsymbol{P}}\} \stackrel{\text{def}}{=} \bar{\boldsymbol{P}} : \bar{\boldsymbol{H}}_\square\{\bar{\boldsymbol{P}}\} - \bar{\psi}_\square\{\bar{\boldsymbol{H}}_\square\{\bar{\boldsymbol{P}}\}\} \tag{3.2.1}$$

Furthermore, we might construct a potential for the stress energy:

$$\Pi^*_\square(\hat{\boldsymbol{u}}, \hat{\boldsymbol{t}}, \hat{\boldsymbol{H}}) \stackrel{\text{def}}{=} \bar{\boldsymbol{P}} : \hat{\boldsymbol{H}} - \langle\psi\rangle_\square + d_\square(\hat{\boldsymbol{t}}, \hat{\boldsymbol{u}}) - d_\square(\hat{\boldsymbol{t}}, \hat{\boldsymbol{H}} \cdot [\boldsymbol{X} - \bar{\boldsymbol{X}}]) \tag{3.2.2}$$

Stationarity of the potential requires that the partial derivatives with respect to $\boldsymbol{u}$, $\boldsymbol{t}$ and $\hat{\boldsymbol{H}}$:

$$\Pi^{*'}_{\square,u}(\boldsymbol{u}, \boldsymbol{t}, \hat{\boldsymbol{H}}; \delta\boldsymbol{u}) = 0 \quad \forall\delta\boldsymbol{u} \in \mathbb{U}_\square \tag{3.2.3}$$

$$\Pi^{*'}_{\square,t}(\boldsymbol{u}, \boldsymbol{t}, \hat{\boldsymbol{H}}; \delta\boldsymbol{t}) = 0 \quad \forall\delta\boldsymbol{t} \in \mathbb{T}_\square \tag{3.2.4}$$

$$\Pi^{*'}_{\square,\hat{H}}(\boldsymbol{u}, \boldsymbol{t}, \hat{\boldsymbol{H}}; \delta\hat{\boldsymbol{H}}) = 0 \quad \forall\delta\hat{\boldsymbol{H}} \in \mathbb{R}_\square \tag{3.2.5}$$

This gives that:

$$a_\square(\boldsymbol{u}; \delta\boldsymbol{u}) - d_\square(\boldsymbol{t}, \delta\boldsymbol{u}) = 0 \quad \forall\delta\boldsymbol{u} \in \mathbb{U}_\square \tag{3.2.6}$$

$$d_\square(\delta\boldsymbol{t}, \boldsymbol{u}) = d_\square(\delta\boldsymbol{t}, \hat{\boldsymbol{H}} \cdot [\boldsymbol{X} - \bar{\boldsymbol{X}}]) \quad \forall\delta\boldsymbol{t} \in \mathbb{T}_\square \tag{3.2.7}$$

$$\bar{\boldsymbol{P}} : \delta\hat{\boldsymbol{H}} = d_\square(\boldsymbol{t}, \delta\hat{\boldsymbol{H}} \cdot [\boldsymbol{X} - \bar{\boldsymbol{X}}]) \quad \forall\delta\hat{\boldsymbol{H}} \in \mathbb{R}^{(3x3)}_\square \tag{3.2.8}$$

These equations are identical to relation $(2.2.15)_1$-$(2.2.15)_3$ in the case of general periodic boundary conditions with stress control, so the choice of potential is correct.

It is possible to write the stress energy in another fashion (which is discussed more in section 3.4.2) according to:

$$\bar{\psi}^*_\square\{\bar{\boldsymbol{P}}\} = \max_{\hat{\boldsymbol{H}} \in \mathbb{R}^{RxR}} \max_{\hat{\boldsymbol{u}} \in \mathbb{U}_\square} \min_{\hat{\boldsymbol{t}} \in \mathbb{T}_\square} \Pi^*_\square(\bar{\boldsymbol{P}}; \hat{\boldsymbol{u}}, \hat{\boldsymbol{t}}, \hat{\boldsymbol{H}}) \tag{3.2.9}$$

Dirichlet and Neumann boundary conditions might be imposed by restricting the function spaces, just as in the previous case of strain energy.

3.3 Fundamental bounds on the energy

As mentioned previous, equation (3.1.6) and (3.2.9) can easily be modified into the case of Dirichlet or Neumann boundary conditions by restricting the function spaces $\mathbb{U}_\square$ and $\mathbb{T}_\square$. So, equation (3.1.6) with Dirichlet boundary conditions yields:

$$\bar{\psi}^D_\square\{\bar{\boldsymbol{H}}\} = \min_{\hat{\boldsymbol{u}} \in \mathbb{U}^D_\square} \max_{\hat{\boldsymbol{t}} \in \mathbb{T}_\square} \Pi_\square(\bar{\boldsymbol{H}}; \hat{\boldsymbol{u}}, \hat{\boldsymbol{t}}) \geqslant \bar{\psi}_\square\{\bar{\boldsymbol{H}}\} \tag{3.3.1}$$

The last inequality can be understood from the following reasoning. $\mathbb{U}^D_\square$ is a subset of $\mathbb{U}_\square$, see Figure 3.3.1. We know that the correct solution is inside $\mathbb{U}_\square$ and will minimize the potential energy. However, the space of admissible displacement functions are restricted and therefore

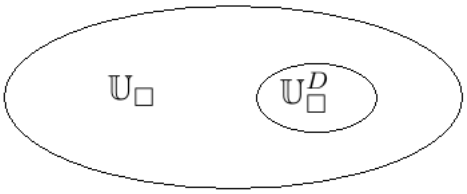

Figure 3.3.1: *The function space* $\mathbb{U}_\square$ *with subset* $\mathbb{U}_\square^D$.

$\bar{\psi}_\square^D$ must be greater than $\bar{\psi}_\square$ or, if the true solution is inside $\mathbb{U}_\square^D$, equal.

If Neumann boundary conditions are imposed, the strain energy might be expressed in the following way:

$$\bar{\psi}_\square^N\{\bar{\boldsymbol{H}}\} = \min_{\hat{\boldsymbol{u}}\in\mathbb{U}_\square} \max_{\hat{\boldsymbol{t}}\in\mathbb{T}_\square^N} \Pi_\square(\bar{\boldsymbol{H}};\hat{\boldsymbol{u}},\hat{\boldsymbol{t}}) \leqslant \bar{\psi}_\square\{\bar{\boldsymbol{H}}\} \tag{3.3.2}$$

The last inequality comes from the fact that we have restricted the function space from where we chose the tractions that should maximize the potential energy but remained the function space from where the displacements that minimizes the problem are chosen.

By the same reasoning as above, it might be concluded that the following two relations hold:

$$\bar{\psi}_\square^{*D}\{\bar{\boldsymbol{P}}\} = \max_{\hat{\boldsymbol{H}}\in\mathbb{R}^{RxR}} \max_{\hat{\boldsymbol{u}}\in\mathbb{U}_\square^D} \min_{\hat{\boldsymbol{t}}\in\mathbb{T}_\square} \Pi_\square^*(\bar{\boldsymbol{P}};\hat{\boldsymbol{u}},\hat{\boldsymbol{t}},\hat{\boldsymbol{H}}) \leqslant \bar{\psi}_\square^*\{\bar{\boldsymbol{P}}\} \tag{3.3.3}$$

$$\bar{\psi}_\square^{*N}\{\bar{\boldsymbol{P}}\} = \max_{\hat{\boldsymbol{H}}\in\mathbb{R}^{RxR}} \max_{\hat{\boldsymbol{u}}\in\mathbb{U}_\square} \min_{\hat{\boldsymbol{t}}\in\mathbb{T}_\square^N} \Pi_\square^*(\bar{\boldsymbol{P}};\hat{\boldsymbol{u}},\hat{\boldsymbol{t}},\hat{\boldsymbol{H}}) \geqslant \bar{\psi}_\square^*\{\bar{\boldsymbol{P}}\} \tag{3.3.4}$$

So, to summarize, for a given RVE the strain and stress energy are bounded by the Dirichlet and Neumann strain and stress energy in the following manner:

$$\bar{\psi}_\square^N\{\bar{\boldsymbol{H}}\} \leqslant \bar{\psi}_\square\{\bar{\boldsymbol{H}}\} \leqslant \bar{\psi}_\square^D\{\bar{\boldsymbol{H}}\} \tag{3.3.5}$$

$$\bar{\psi}_\square^{*D}\{\bar{\boldsymbol{P}}\} \leqslant \bar{\psi}_\square^*\{\bar{\boldsymbol{P}}\} \leqslant \bar{\psi}_\square^{*N}\{\bar{\boldsymbol{P}}\} \tag{3.3.6}$$

It should be noted that the relation between the stress and strain energy can be expressed as below via Legendre transformations.

$$\bar{\psi}_\square^*\{\bar{\boldsymbol{P}}\} = \max_{\hat{\boldsymbol{H}}\in\mathbb{R}^{3x3}} [\bar{\boldsymbol{P}} : \hat{\boldsymbol{H}} - \bar{\psi}_\square\{\hat{\boldsymbol{H}}\}] \tag{3.3.7}$$

$$\bar{\psi}_\square\{\bar{\boldsymbol{H}}\} = \max_{\hat{\boldsymbol{P}}\in\mathbb{R}^{3x3}} [\hat{\boldsymbol{P}} : \bar{\boldsymbol{H}} - \bar{\psi}_\square^*\{\hat{\boldsymbol{P}}\}] \tag{3.3.8}$$

3.4 Computable bounds on the strain energy

As been mentioned earlier, it is expected that the influence of the boundary conditions will vanish as the size of the RVE approaches infinity, i.e:

$$\bar{\psi}\{\bar{\boldsymbol{H}}\} \overset{\text{def}}{=} \lim_{|\Omega_\square|\to\infty} \bar{\psi}_\square\{\bar{\boldsymbol{H}}\} = \lim_{|\Omega_\square|\to\infty} \bar{\psi}_\square^D\{\bar{\boldsymbol{H}}\} = \lim_{|\Omega_\square|\to\infty} \bar{\psi}_\square^N\{\bar{\boldsymbol{H}}\} \tag{3.4.1}$$

$$\bar{\psi}^*\{\bar{\boldsymbol{P}}\} \overset{\text{def}}{=} \lim_{|\Omega_\square|\to\infty} \bar{\psi}_\square^*\{\bar{\boldsymbol{P}}\} = \lim_{|\Omega_\square|\to\infty} \bar{\psi}_\square^{*D}\{\bar{\boldsymbol{P}}\} = \lim_{|\Omega_\square|\to\infty} \bar{\psi}_\square^{*N}\{\bar{\boldsymbol{P}}\} \tag{3.4.2}$$

However, it is practically impossible to use an infinitely large RVE and therefore we aim for determining upper and lower bounds on $\bar{\psi}\{\bar{\boldsymbol{H}}\}$ and $\bar{\psi}^*\{\bar{\boldsymbol{P}}\}$. Since the strain and stress energies are related to each other according to equation (3.3.7) and (3.3.8), it is enough to derive bounds for one of them. In this study the focus is set on the strain energy. The following two subsections will discuss how to obtain computable upper and lower bounds on the strain energy.

3.4.1 Upper bound on the strain energy

If a certain realization of a RVE, $\Omega_{(\square)}$, is considered, it might be divided into N sub RVEs, $\Omega_{\square,i}$ according to Figure 3.4.1.

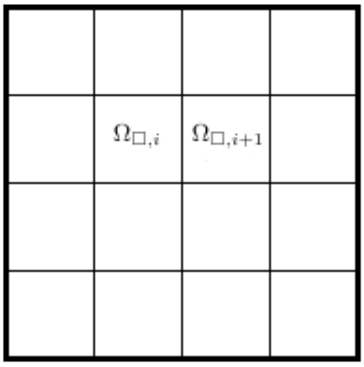

Figure 3.4.1: *The RVE realization $\Omega_{(\square)}$ divided into N $\Omega_{\square,i}$ sub RVEs.*

It is possible to introduce further restrictions on the admissible test functions by introducing a new function space:

$$\hat{\mathbb{U}}^D_{(\square)}(\bar{\boldsymbol{H}}) = \{\boldsymbol{u} \in \mathbb{U}^D_{(\square)}(\bar{\boldsymbol{H}}) : \boldsymbol{u} = \bar{\boldsymbol{H}} \cdot [\boldsymbol{X} - \bar{\boldsymbol{X}}] \text{ on each } \partial\Omega_{\square,i}\} \subset \mathbb{U}^D_{(\square)}(\bar{\boldsymbol{H}}) \tag{3.4.3}$$

If the new function space is used in equation (3.1.6) the following inequalities are obtained:

$$\begin{aligned}\bar{\psi}_{(\square)}\{\bar{\boldsymbol{H}}\} \leqslant \min_{\hat{\boldsymbol{u}} \in \mathbb{U}^D_{(\square)}(\bar{\boldsymbol{H}})} \Pi^D_{(\square)}(\hat{\boldsymbol{u}}) \leqslant \min_{\hat{\boldsymbol{u}} \in \hat{\mathbb{U}}^D_{(\square)}(\bar{\boldsymbol{H}})} \Pi^D_{(\square)}(\hat{\boldsymbol{u}}) = \\ = \frac{1}{N}\sum_{i=1}^{N} \min_{\hat{\boldsymbol{u}} \in \mathbb{U}^D_{\square,i}(\bar{\boldsymbol{H}})} \Pi^D_{\square,i}(\hat{\boldsymbol{u}}) = \frac{1}{N}\sum_{i=1}^{N} \bar{\psi}^D_{\square,i}\{\bar{\boldsymbol{H}}\}\end{aligned} \tag{3.4.4}$$

where $\Pi^D_{(\square)}(\hat{\boldsymbol{u}}) = \langle \psi(\bar{\boldsymbol{H}}[\hat{\boldsymbol{u}}]) \rangle_\square$. The second inequality comes from the fact that the function is minimized over a smaller function space. It is now possible to reformulate equation (3.4.1) in the following way:

$$\bar{\psi}\{\bar{\boldsymbol{H}}\} = \lim_{|\Omega_{(\square)}| \to \infty} \bar{\psi}_\square\{\bar{\boldsymbol{H}}\} = \lim_{|\Omega_{(\square)}| \to \infty} \bar{\psi}^D_\square\{\bar{\boldsymbol{H}}\} \leqslant \lim_{|\Omega_{(\square)}| \to \infty} \frac{1}{N}\sum_{i=1}^{N} \bar{\psi}^D_{\square,i}\{\bar{\boldsymbol{H}}\} \tag{3.4.5}$$

Note that the size of each $\Omega_{\square,i}$ is fixed and of finite size even if the size of $\Omega_{(\square)}$ approaches infinity. The last term can be developed further:

$$\lim_{|\Omega_{(\square)}|\to\infty} \frac{1}{N}\sum_{i=1}^{N} \bar{\psi}^D_{\square,i}\{\bar{\boldsymbol{H}}\} = \{\text{Fixed } \mid \Omega_{\square,i} \mid \Rightarrow N \to \infty \text{ as } \mid \Omega_{(\square)} \mid \to \infty\} =$$

$$= \lim_{N\to\infty} \frac{1}{N}\sum_{i=1}^{N} \bar{\psi}^D_{\square,i}\{\bar{\boldsymbol{H}}\} = \lim_{N\to\infty} \frac{1}{N}\sum_{i=1}^{N} \bar{\psi}^D_{\square}\{\bar{\boldsymbol{H}},\omega_i\} = E[\bar{\psi}^D_{\square}\{\bar{\boldsymbol{H}},\tilde{\omega}\}] \tag{3.4.6}$$

where E is the expected value and ω_i is one realization of the stochastic process $\tilde{\omega}$, which determine the properties of the RVE. The last equality says that studying N different sub RVEs of one realization is equivalent to study N realizations of one RVE. This holds if $\tilde{\omega}$ is ergodic. To summary, we have that:

$$\bar{\psi}\{\bar{\boldsymbol{H}}\} \leqslant E[\bar{\psi}^D_{\square}\{\bar{\boldsymbol{H}},\tilde{\omega}\}] \tag{3.4.7}$$

In practice it is impossible to compute the true expected value above. However, a sample mean value, μ, can be calculated and for that mean value a confidence interval, c, of confidence $\bar{P}$ might be constructed. Therefore equation (3.4.7) can be developed further:

$$\bar{\psi}\{\bar{\boldsymbol{H}}\} \leqslant E[\bar{\psi}^D_{\square}\{\bar{\boldsymbol{H}},\tilde{\omega}\}] \leqslant \mu[\bar{\psi}^D_{\square}\{\bar{\boldsymbol{H}},\omega_i\}^N_{i=1}] + c[\bar{\psi}^D_{\square}\{\bar{\boldsymbol{H}},\omega_i\},\bar{P}] \stackrel{\text{def}}{=} \bar{\psi}^{UB}_{\square}\{\bar{\boldsymbol{H}}\} \tag{3.4.8}$$

where $\bar{\psi}^{UB}_{\square}\{\bar{\boldsymbol{H}}\}$ is the computable upper bound of the strain energy.

Note that the following denotations sometimes are used:

$$\bar{\psi}^{D-V(\infty)}_{\square} = E[\bar{\psi}^D_{\square}\{\bar{\boldsymbol{H}};\tilde{\omega}\}] \tag{3.4.9}$$

$$\bar{\psi}^{D-V(N)}_{\square} = \mu[\bar{\psi}^D_{\square}\{\bar{\boldsymbol{H}},\omega_i\}^N_{i=1}] \tag{3.4.10}$$

where V means Voigt sampling. The classical Voigt bound is defined as follows:

$$\bar{\psi}^V = \lim_{|\Omega_{(\square)}|\to 0} \bar{\psi}^{D-V(\infty)}_{\square}\{\bar{\boldsymbol{H}}\} = \lim_{|\Omega_{(\square)}|\to 0} \bar{\psi}^{N-V(\infty)}_{\square}\{\bar{\boldsymbol{H}}\} = n\psi_{inc}(\bar{\boldsymbol{H}}) + (1-n)\psi_{mat}(\bar{\boldsymbol{H}}) \tag{3.4.11}$$

where n is the theoretical volume fraction, ψ_{inc} is the strain energy in the inclusion material and ψ_{mat} is the strain energy in the matrix material.

3.4.2 Lower bound on the strain energy

The next task is to derive an expression for the lower bound on the strain energy. It turns out that it is not as straight forward as in the case of the upper bound. We begin by conclude that for a finite RVE, $\Omega_{\square}$, we can use equation (3.3.7) and the expression for the strain energy in equation (3.1.6) to obtain the following expression:

$$\bar{\psi}^*_{\square}\{\bar{\boldsymbol{P}}\} = \max_{\hat{\boldsymbol{H}}\in\mathbb{R}^{3x3}_{\square}} [\bar{\boldsymbol{P}} : \hat{\boldsymbol{H}} - \bar{\psi}_{\square}\{\hat{\boldsymbol{H}}\}] = \max_{\hat{\boldsymbol{H}}\in\mathbb{R}^{3x3}} \max_{\hat{\boldsymbol{u}}\in\mathbb{U}_{\square}} \min_{\hat{\boldsymbol{t}}\in\mathbb{T}_{\square}} \Pi^*_{\square}(\bar{\boldsymbol{P}};\hat{\boldsymbol{H}},\hat{\boldsymbol{u}},\hat{\boldsymbol{t}}) \tag{3.4.12}$$

where the stress energy potential is defined as before, which is identical to equation (3.2.9), but now motivated.

As in the case of the upper bounds, we construct a "super-RVE", $\Omega_{(\square)}$, consisting of small RVEs of fixed size $\Omega_\square$. Now we are able to study the energy stress in the following way:

$$\bar{\psi}^*_{(\square)}\{\bar{\boldsymbol{P}}\} = \max_{\hat{\boldsymbol{H}}\in\mathbb{R}^{3x3}} [\bar{\boldsymbol{P}} : \hat{\boldsymbol{H}} - \bar{\psi}_{(\square)}\{\hat{\boldsymbol{H}}\}] =$$
$$\max_{\hat{\boldsymbol{H}}\in\mathbb{R}^{3x3}} \max_{\hat{\boldsymbol{u}}\in\mathbb{U}_{(\square)}} \min_{\hat{\boldsymbol{t}}\in\mathbb{T}_{(\square)}} [\bar{\boldsymbol{P}} : \hat{\boldsymbol{H}} - \langle\psi\rangle_{(\square)} - \frac{1}{\mid \Omega_{(\square)} \mid} \int_{\Gamma^+_{(\square)}} [\![\hat{\boldsymbol{u}} - \hat{\boldsymbol{H}} \cdot [\boldsymbol{X} - \bar{\boldsymbol{X}}]]\!] \cdot \hat{\boldsymbol{t}} d\Gamma] \tag{3.4.13}$$

We can now replace the continuity by inserting the Lagrange multiplyers $\hat{\boldsymbol{t}} \in \bar{\mathbb{T}}_{(\square)}$, where

$$\bar{\mathbb{T}}_{(\square)} = \{\boldsymbol{t} \text{ sufficiently regular on } (\cup\partial\Omega_\square) \setminus \Gamma^-_{(\square)}\} \tag{3.4.14}$$

The resulting expression is:

$$\bar{\psi}^*_{(\square)}\{\bar{\boldsymbol{P}}\} = \max_{\hat{\boldsymbol{H}}\in\mathbb{R}^{3x3}} \max_{\hat{\boldsymbol{u}}\in\check{\mathbb{U}}_{(\square)}} \min_{\hat{\boldsymbol{t}}\in\bar{\mathbb{T}}_{(\square)}} [\bar{\boldsymbol{P}} : \hat{\boldsymbol{H}} - \langle\psi\rangle_{(\square)} - \frac{1}{\mid \Omega_{(\square)} \mid} \int_{\Gamma^+_{(\square)}} [\![\hat{\boldsymbol{u}} - \hat{\boldsymbol{H}} \cdot [\boldsymbol{X} - \bar{\boldsymbol{X}}]]\!] \cdot \hat{\boldsymbol{t}} d\Gamma$$
$$- \frac{1}{\mid \Omega_\square \mid} \int_{\Gamma_{int}} [\![\hat{\boldsymbol{u}}]\!] \cdot \hat{\boldsymbol{t}} d\Gamma] \tag{3.4.15}$$

where $\Gamma_{int} = \cup\partial\Omega_\square \setminus (\Gamma^+_{(\square)} \cup \Gamma^-_{(\square)})$ and the expanded displacement space is

$$\check{\mathbb{U}}_{(\square)} = \{\boldsymbol{u}|_{\Omega_{\square,i}} \in \check{\mathbb{U}}_{\square,i}\} \tag{3.4.16}$$

where $\check{\mathbb{U}}_{\square,i}$ is the space of sufficiently regular functions on each $\Omega_{\square,i}$. Note that the only difference between $\mathbb{U}_{\square,i}$ and $\check{\mathbb{U}}_{\square,i}$ are rigid body translation, which do not effect neither $\langle\boldsymbol{H}\rangle$ or $\langle\psi\rangle$. On each Γ_{int} we define a unique normal $\boldsymbol{N}$ and define the jump over the boundaries $[\![\boldsymbol{u}]\!] = \boldsymbol{u}^+ - \boldsymbol{u}^-$. This is illustrated in Figure 3.4.2. Also note that $\bar{\mathbb{T}}_{(\square)}$ contain the tractions in $\mathbb{T}_{(\square)}$ too.

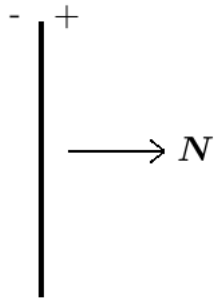

Figure 3.4.2: *The figure shows the meaning of the jump over the internal boundaries of* $\Omega_{(\square)}$ *as well as a normal direction.*

If we use the restriction $\hat{\bar{\mathbb{T}}}_{(\square)} \subset \bar{\mathbb{T}}_{(\square)}$ defined as:

$$\hat{\bar{\mathbb{T}}}_{(\square)} = \{\hat{\boldsymbol{t}} = \hat{\boldsymbol{P}} \cdot \boldsymbol{N} \text{ for constant } \hat{\boldsymbol{P}} \in \mathbb{R}^{3x3}\} \tag{3.4.17}$$

we obtain:

$$\bar{\psi}^{*}_{(\square)}\{\bar{\boldsymbol{P}}\} \leqslant \max_{\hat{\boldsymbol{H}}\in\mathbb{R}^{3x3}} \max_{\hat{\boldsymbol{u}}\in\check{\mathbb{U}}_{(\square)}} \min_{\hat{\boldsymbol{P}}\in\mathbb{R}^{3x3}} [\bar{\boldsymbol{P}} : \hat{\boldsymbol{H}} - \langle\psi\rangle_{(\square)} - \frac{1}{\mid\Omega_{(\square)}\mid}\int_{\Gamma^{+}_{(\square)}} [\![\hat{\boldsymbol{u}} - \hat{\boldsymbol{H}}\cdot[\boldsymbol{X}-\bar{\boldsymbol{X}}]]\!]\cdot\hat{\boldsymbol{P}}\cdot\boldsymbol{N}d\Gamma$$

$$-\frac{1}{\mid\Omega_{(\square)}\mid}\int_{\Gamma_{int}} [\![\hat{\boldsymbol{u}}]\!]\cdot\hat{\boldsymbol{P}}\cdot\boldsymbol{N}d\Gamma] = \max_{\hat{\boldsymbol{H}}\in\mathbb{R}^{3x3}} \max_{\hat{\boldsymbol{u}}\in\check{\mathbb{U}}_{(\square)}} \min_{\hat{\boldsymbol{P}}\in\mathbb{R}^{3x3}} [\bar{\boldsymbol{P}} : \hat{\boldsymbol{H}} + \hat{\boldsymbol{P}} : \hat{\boldsymbol{H}} - \sum_{i=1}^{N}\frac{\mid\Omega_{\square}\mid}{\mid\Omega_{(\square)}\mid}\langle\psi\rangle_{\square,i} -$$

$$\sum_{i=1}^{N}\hat{\boldsymbol{P}} : \frac{1}{\mid\Omega_{(\square)}\mid}\int_{\Gamma_{\square,i}}\hat{\boldsymbol{u}}\otimes\boldsymbol{N}d\Gamma] =$$

$$\{\hat{\boldsymbol{H}} = \frac{1}{N}\sum_{i=1}^{N}\langle\boldsymbol{H}[\hat{\boldsymbol{u}}]\rangle_{\square,i} \text{ and } \frac{1}{\mid\Omega_{(\square)}\mid}\int_{\Gamma_{\square,i}}\hat{\boldsymbol{u}}\otimes\boldsymbol{N}d\Gamma = \frac{\mid\Omega_{\square}\mid}{\mid\Omega_{(\square)}\mid}\langle\boldsymbol{H}[\hat{\boldsymbol{u}}]\rangle_{\square,i}\} =$$

$$\max_{\hat{\boldsymbol{u}}\in\check{\mathbb{U}}_{(\square)}}[\frac{1}{N}\sum_{i=1}^{N}(\bar{\boldsymbol{P}} : \langle\boldsymbol{H}[\hat{\boldsymbol{u}}]\rangle_{\square,i} - \langle\psi\rangle_{\square,i})] = \frac{1}{N}\sum_{i=1}^{N}\max_{\hat{\boldsymbol{u}}_i\in\check{\mathbb{U}}_{\square,i}}[\bar{\boldsymbol{P}} : \langle\boldsymbol{H}[\hat{\boldsymbol{u}}_i]\rangle_{\square,i} - \langle\psi\rangle_{\square,i}] = \frac{1}{N}\sum_{i=1}^{N}\bar{\psi}^{*N}_{\square,i}\{\bar{\boldsymbol{P}}\} \tag{3.4.18}$$

So, in summary we can, with help of the same reasoning as for the upper bound regarding an infinitely large RVE, conclude that:

$$\bar{\psi}^{*}\{\bar{\boldsymbol{P}}\} = \lim_{|\Omega_{\square}|\to\infty}\bar{\psi}^{*}_{\square}\{\bar{\boldsymbol{P}}\} \leqslant \lim_{|\Omega_{\square}|\to\infty}\frac{1}{N}\sum_{i=1}^{N}\bar{\psi}^{*N}_{\square,i}\{\bar{\boldsymbol{P}}\} =$$

$$\lim_{N\to\infty}\frac{1}{N}\sum_{i=1}^{N}\bar{\psi}^{*N}_{\square,i}\{\bar{\boldsymbol{P}}\} = E[\bar{\psi}^{*N}_{\square}\{\bar{\boldsymbol{P}}\}] \tag{3.4.19}$$

Therefore, with help of (3.3.8), it must follow that the following expression holds:

$$\bar{\psi}\{\bar{\boldsymbol{H}}\} = \max_{\hat{\boldsymbol{P}}\in\mathbb{R}^{3x3}}[\hat{\boldsymbol{P}} : \bar{\boldsymbol{H}} - \bar{\psi}^{*}\{\hat{\boldsymbol{P}}\}] \geqslant \max_{\hat{\boldsymbol{P}}\in\mathbb{R}^{3x3}}[\hat{\boldsymbol{P}} : \bar{\boldsymbol{H}} - E[\bar{\psi}^{*N}_{\square}\{\hat{\boldsymbol{P}}\}]] \geqslant$$

$$\max_{\hat{\boldsymbol{P}}\in\mathbb{R}^{3x3}}[\hat{\boldsymbol{P}} : \bar{\boldsymbol{H}} - \mu[\bar{\psi}^{*N}_{\square}\{\hat{\boldsymbol{P}}\}] - c[\bar{\psi}^{*N}_{\square}\{\hat{\boldsymbol{P}}\}, \bar{P}]] \geqslant$$

$$\tilde{\hat{\boldsymbol{P}}} : \bar{\boldsymbol{H}} - \mu[\bar{\psi}^{*N}_{\square}\{\tilde{\hat{\boldsymbol{P}}}, \tilde{\omega}_i\}^{N}_{i=1}] - c[\bar{\psi}^{*N}_{\square}\{\tilde{\hat{\boldsymbol{P}}}, \tilde{\omega}_i\}^{N}_{i=1}, \bar{P}] \overset{\text{def}}{=} \bar{\psi}^{LB}_{\square}\{\bar{\boldsymbol{H}}\} \tag{3.4.20}$$

where $\tilde{\hat{\boldsymbol{P}}} \in \mathbb{R}^{3x3}$ is arbitrary. This means that any choice of $\tilde{\hat{\boldsymbol{P}}}$ will result in a lower bound, but it is of course of interest to chose the $\tilde{\hat{\boldsymbol{P}}}$ that results in the largest possible $\bar{\psi}^{LB}_{\square}(\bar{\boldsymbol{H}})$ in order to get sharp bounds on the strain energy. Therefore $\tilde{\hat{\boldsymbol{P}}}$ could be obtained in the following (optimal) manner:

$$\tilde{\hat{\boldsymbol{P}}} = \arg\max_{\hat{\boldsymbol{P}}\in\mathbb{R}^{3x3}}[\hat{\boldsymbol{P}} : \bar{\boldsymbol{H}} - \mu[\bar{\psi}^{*N}_{\square}\{\hat{\boldsymbol{P}}, \tilde{\omega}_i\}^{N}_{i=1}] - c[\bar{\psi}^{*N}_{\square}\{\hat{\boldsymbol{P}}, \tilde{\omega}_i\}^{N}_{i=1}, \bar{P}]] \tag{3.4.21}$$

Larsson et al. [6] also suggest a "quasi-optimal" choice of $\tilde{\hat{\boldsymbol{P}}}$ in the following way:

$$\tilde{\hat{\boldsymbol{P}}} = \arg\max_{\hat{\boldsymbol{P}}\in\mathbb{R}^{3x3}}[\hat{\boldsymbol{P}} : \bar{\boldsymbol{H}} - \mu[\bar{\psi}^{*N}_{\square}\{\hat{\boldsymbol{P}}, \tilde{\omega}_i\}^{N}_{i=1}]] \tag{3.4.22}$$

which of course is the optimal choice as $c \to 0$.

Note that the following denotations sometimes are used:

$$\bar{\psi}_{\square}^{N-R(\infty)}\{\bar{\boldsymbol{H}}\} = \max_{\hat{\boldsymbol{P}} \in \mathbb{R}^{3x3}} [\hat{\boldsymbol{P}} : \bar{\boldsymbol{H}} - E[\bar{\psi}_{\square}^{*N}\{\hat{\boldsymbol{P}}\}]] \tag{3.4.23}$$

$$\bar{\psi}_{\square}^{N-R(N)}\{\bar{\boldsymbol{H}}\} = \max_{\hat{\boldsymbol{P}} \in \mathbb{R}^{3x3}} [\hat{\boldsymbol{P}}\{\bar{\boldsymbol{H}}\} : \bar{\boldsymbol{H}} - \mu[\bar{\psi}_{\square}^{*N}\{\hat{\boldsymbol{P}}\{\bar{\boldsymbol{H}}\}, \tilde{\omega}_i\}_{i=1}^{N}] \tag{3.4.24}$$

where R means Reuss sampling. The classical Reuss bound is defined as follows:

$$\bar{\psi}^{R} = \lim_{|\Omega_{(\square)}| \to 0} \bar{\psi}_{\square}^{D-R(\infty)}\{\bar{\boldsymbol{H}}\} = \lim_{|\Omega_{(\square)}| \to 0} \bar{\psi}_{\square}^{N-R(\infty)}\{\bar{\boldsymbol{H}}\} = \max_{\hat{\boldsymbol{P}} \in \mathbb{R}^{3x3}} [\hat{\boldsymbol{P}} : \bar{\boldsymbol{H}} - n\bar{\psi}_{inc}^{*}(\hat{\boldsymbol{P}}) - (1-n)\bar{\psi}_{mat}^{*}(\hat{\boldsymbol{P}})] \tag{3.4.25}$$

where ψ_{inc}^{*} is the stress energy in the inclusion material and ψ_{mat}^{*} is the stress energy in the matrix material.

4 Virtual testing

The following section describes how the virtual testing was performed. In order to avoid unnecessary computational difficulties, only two dimensional problems were considered. This resulted in that volume integrals from the general theory were replaced by surface integrals, volume fractions with area fractions etc. Furthermore, only circular inclusions were considered. Beside this, all virtual tests were strain driven.

4.1 The RVE generator

In order to perform proper virtual tests with RVEs the issue of RVE generation is of course important. In this study, the following parameters were prescribed: The volume fraction, V_f (inclusion volume/total volume), standard deviation of the inclusion radius, $std[R]$, V_p (total volume/number of inclusions), and window size, $l_\square$. The aim was then to generate RVEs in such a way that the prescribed volume fraction, in average, would be retrieved. To avoid difficulties regarding the implementation of periodic boundaries, a large RVE was generated from where the window was centered in the middle on a offset distance R_{max}, see Figure 4.1.1. The reason for introducing the offset distance was to ensure that no inclusion on a $L_\square$-boundary would affect the window.

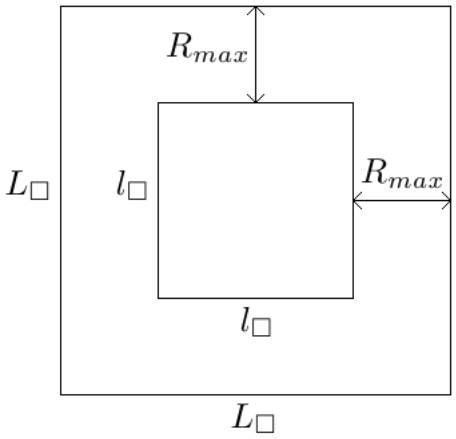

Figure 4.1.1: *The figure shows $L_\square$, $l_\square$ and R_{max}.*

In order to implement this system in practice, a number of variables had to be computed. The list below shows how this was done.

1. V_f, $std[R]$, V_p and $l_\square$ were chosen.
2. Given V_f, $std[R]$ and V_p the expected value of the inclusion radius, $E[R]$, could be computed.
3. Given $E[R]$ and $std[R]$, the offset distance R_{max} could be computed in such a way that no boundary inclusion would affect the window.

4. Given R_{max} and V_p, the needed number of inclusions, N, could be computed.

5. Given N and V_p, the size of the large RVE, $L_\square$, could finally be determined.

When the variables above had been calculated, N number of inclusions with radius $E[R]$ was randomly placed on a RVE of size $L_\square \times L_\square$. The inclusions were not allowed to overlap each other. Then a window of size $l_\square \times l_\square$ was chosen and meshed. The window then become the new RVE on which the actual computations took place.

4.2 The mesh

The RVEs were meshed with constant strain triangles in such a way that the boundaries of the inclusions were accounted for, see Figure 4.2.1. The main problem regarding the mesh size was to obtain a mesh with a resolution good enough not to influence the volume fraction but coarse enough to avoid a unnecessarily high computation cost.

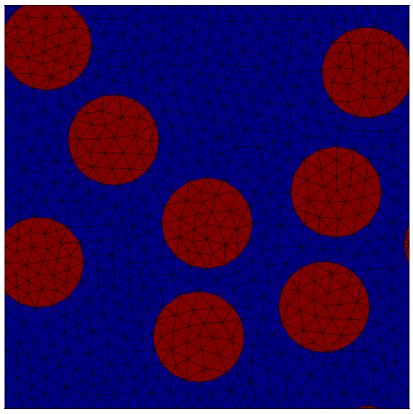

Figure 4.2.1: *A typical RVE with a triangular mesh. The red part of the figure represents circular inclusions while the blue part represents matrix material.*

4.3 The constitutive model

In this study it was of interest to simulate a material with a linear hardening behavior. Therefore the aim was to use a (strain driven) constitutive model that could generate stresses and strain energy. One usual way of doing this is to use a model based on incremental theory with internal variables. However, this would lead to unnecessary complexity, and in order to simplify things a model based on the strain only (i.e. a type of elasticity model or a single step of an incremental based theory) was used. The disadvantage of this type of theory is that no study of unloading is possible, which implicate that no cyclic behavior could be modeled, but only monotonically increasing stress.

The strain energy per unit volume might then be calculated as below:

$$\psi(\boldsymbol{H}) = \psi^{iso}(H_e^{vM}) + \psi^{vol}(H_{vol}) \tag{4.3.1}$$

where $H_e^{vM} = \sqrt{\frac{2}{3}} \mid\mid \boldsymbol{H}_{dev}^{sym} \mid\mid$. $\boldsymbol{H}_{dev}^{sym}$ is the deviatoric part of the symmetric part of $\boldsymbol{H}$ and H_{vol} is the volumetric part of $\boldsymbol{H}$. Furthermore,

$$\psi^{iso}(H_e^{vM}) = \begin{cases} \frac{3G}{2}(H_e^{vM}) & \text{if } H_e^{vM} \leq \frac{\sigma_y}{3G} \\ \frac{\sigma_y^2}{6G}(h/G-1) + \sigma_y(1-h/G)H_e^{vM} + \frac{3h}{2}(H_e^{vM})^2 & \text{if } H_e^{vM} > \frac{\sigma_y}{3G} \end{cases}$$

$$\psi^{vol}(H_{vol}) = \frac{1}{2}KH_{vol}^2$$

where h is a parameter related to the hardening, σ_y is the yield limit, $G = \frac{E}{2(1+\nu)}$, $K = \frac{E}{3(1-2\nu)}$, E is the Youngs modulus and ν is Poissons ratio. A local constitutive model like this produces a strain energy vs. strain curve according to Figure 4.3.1.

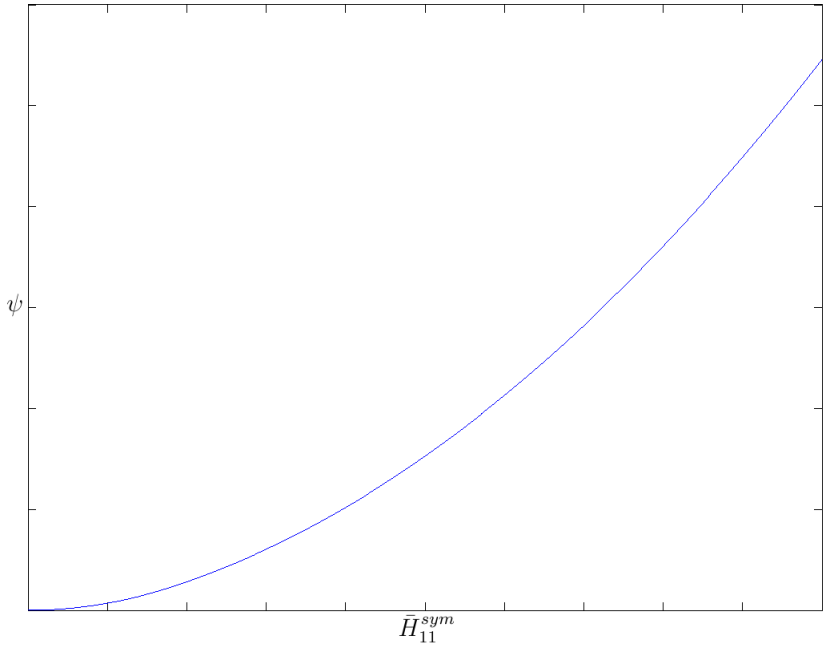

Figure 4.3.1: *The principal look of a strain vs. strain energy plot.*

According to the fact that $\boldsymbol{P}(\boldsymbol{H}) = \frac{\partial \psi(\boldsymbol{H})}{\partial \boldsymbol{H}}$ the expressions above yield, after some manipulations, that the following expression must hold for the stress:

$$\boldsymbol{P}(\boldsymbol{H}) = 2G^*(H_e^{vM})\boldsymbol{H}_{dev}^{sym} + KH_{vol}\boldsymbol{I} \tag{4.3.2}$$

where

$$G^*(H_e^{vM}) = \begin{cases} G & \text{if } H_e^{vM} \leq \frac{\sigma_y}{3G} \\ \frac{\sigma_y(1-h/G)}{3H_e^{vM}} + h & \text{if } H_e^{vM} > \frac{\sigma_y}{3G} \end{cases}$$

The typical look of this kind of local constitutive model is showed in Figure 4.3.2. Note that even if the microscale stress strain relation results in a sharp wedge in the curve, the homogenized response will be smooth.

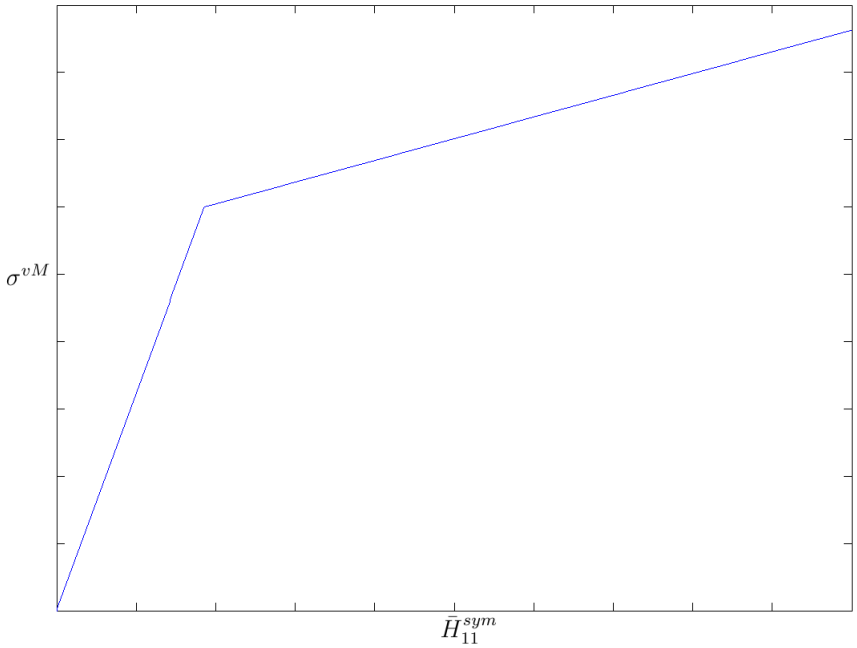

Figure 4.3.2: *The symmetric deformation gradient vs. the von Mises-stress.*

4.4 Choice of $\tilde{\bar{\boldsymbol{P}}}$

As been mentioned earlier, the choice of $\tilde{\bar{\boldsymbol{P}}}$ is an important issue when calculating the lower bound of the strain energy. Equations (3.4.21) and (3.4.22) suggested two methods. Equation (3.4.21) offers considerable computational difficulties, regardless of the choice of material model (even for linear elasticity), while equation (3.4.22) is straight-forward for the case of linear elasticity.

Another method was used to construct $\tilde{\bar{\boldsymbol{P}}}$. The following equation holds true by definition:

$$\bar{\psi}_{\square}^{N-R(N)}\{\bar{\boldsymbol{H}}\} = \max_{\hat{\boldsymbol{P}}}[\hat{\boldsymbol{P}} : \bar{\boldsymbol{H}} - \mu[\bar{\psi}_{\square}^{*N}\{\hat{\boldsymbol{P}}\}]] = \max_{\hat{\boldsymbol{P}}}[\hat{\boldsymbol{P}} : \bar{\boldsymbol{H}} - \mu[\max_{\hat{\boldsymbol{H}}}[\hat{\boldsymbol{P}} : \hat{\boldsymbol{H}} - \bar{\psi}_{\square}^{N}\{\hat{\boldsymbol{H}}\}]]] \tag{4.4.1}$$

If we now assume that $\hat{\boldsymbol{H}}$ is the same for all realizations, which is the case if the RVEs are similar, we can continue the derivation in the following manner:

$$\max_{\hat{\boldsymbol{P}}}[\hat{\boldsymbol{P}} : \bar{\boldsymbol{H}} - \mu[\max_{\hat{\boldsymbol{H}}}[\hat{\boldsymbol{P}} : \hat{\boldsymbol{H}} - \bar{\psi}_{\square}^{N}\{\hat{\boldsymbol{H}}\}]]] \approx \max_{\hat{\boldsymbol{P}}}[\hat{\boldsymbol{P}} : \bar{\boldsymbol{H}} - \max_{\hat{\boldsymbol{H}}}[\hat{\boldsymbol{P}} : \hat{\boldsymbol{H}} - \mu[\bar{\psi}_{\square}^{N}\{\hat{\boldsymbol{H}}\}]]] = \max_{\hat{\boldsymbol{P}}}\min_{\hat{\boldsymbol{H}}}[\hat{\boldsymbol{P}} : \bar{\boldsymbol{H}} - \hat{\boldsymbol{P}} : \hat{\boldsymbol{H}} + \mu[\bar{\psi}_{\square}^{N}\{\hat{\boldsymbol{H}}\}]] \tag{4.4.2}$$

Variation with respect to $\hat{\boldsymbol{H}}$ infers that $\hat{\boldsymbol{P}} = \mu[\bar{\boldsymbol{P}}_{\square}^{N}\{\hat{\boldsymbol{H}}\}]$ and variation with respect to $\hat{\boldsymbol{P}}$ infers that $\hat{\boldsymbol{H}} = \bar{\boldsymbol{H}}$.

Therefore $\bar{\bar{\boldsymbol{P}}}$ can be approximated by the sample mean of the stress from a strain-driven Neumann problem:

$$\bar{\bar{\boldsymbol{P}}} = \mu[\bar{\boldsymbol{P}}^N_\square\{\bar{\boldsymbol{H}}\}] \approx \arg \max_{\hat{\boldsymbol{P}} \in \mathbb{R}^{3x3}} [\hat{\boldsymbol{P}} : \bar{\boldsymbol{H}} - \mu[\bar{\psi}^{*N}_\square\{\hat{\boldsymbol{P}}, \tilde{\omega}_i\}_{i=1}^N]] \tag{4.4.3}$$

As mentioned above, this choice will also result in a lower bound on the strain energy, but in general it will not produce as tight bound as if the optimal choice-method would have been used.

4.5 Strategy for obtaining stress-strain relation

Given a full strain energy versus strain relation, where the upper and lower bounds of the strain energy has been calculated for a number of strains it is desirable to construct a full stress-strain relation. Several more or less accurate options are available, but only one is considered in this study. It is based on that the effective properties $\bar{E}, \bar{\nu}, \bar{h}, \bar{\sigma}_y$ are determined in such a way that the macroscopic strain response they produce fit the upper and lower bounds optimally. The method is described in more detail below.

Given the upper and lower bounds of the strain energy a mid-curve, $\bar{\bar{\psi}}_\square$ might be constructed:

$$\bar{\bar{\psi}}_\square = \frac{\bar{\psi}^{UB}_\square + \bar{\psi}^{LB}_\square}{2} \tag{4.5.1}$$

According to the constitutive model, it is possible to construct a macroscopic strain energy response given $\bar{E}, \bar{\nu}, \bar{h}, \bar{\sigma}_y$ and $\bar{\boldsymbol{H}}$. The effective properties can then be found by using the least squares method, i.e. searching for parameters that minimize the distance between the macroscale response and the mid-curve:

$$\{\bar{E}, \bar{\nu}, \bar{h}, \bar{\sigma}_y\} = \arg \min_{\hat{E}, \hat{\nu}, \hat{h}, \hat{\sigma}_y} \sum_i^N \frac{1}{2}[\bar{\bar{\psi}}_\square(\bar{\boldsymbol{H}}_i) - \bar{\psi}(\hat{E}, \hat{\nu}, \hat{h}, \hat{\sigma}_y; \bar{\boldsymbol{H}}_i)]^2 \tag{4.5.2}$$

where N is the number of strain increments.

When the optimal parameters are found, these can be used in the constitutive model to construct the corresponding strain energy curve, here called $\bar{\psi}^{expl}$ where "expl" denotes "explicit". However, it is unknown how good this estimation really is. Therefore the corresponding strain energy and stress for that RVE, for which the strain energy is closest to $\bar{\bar{\psi}}_\square$ in a least squares sense, is investigated and compared with $\bar{\psi}^{expl}$. This is further discussed and presented with some numerical results in Section 5.3.

5 Numerical results

This chapter will present some numerical results based on the computational strategies described previously.

5.1 Convergence of upper and lower bounds

Figure 5.1.1 shows how the upper and lower bounds, $\bar{\psi}_{\square}^{UB}$ and $\bar{\psi}_{\square}^{LB}$, change with the size of the RVE, $L_{\square}$ for a given deformation gradient. The upper solid line represents the sample mean value from equation (3.4.8) while the upper dashed line represents the confidence from the same equation. The lower solid line corresponds to the two first terms of the lower bound of equation (3.4.20) and the lower dashed line corresponds to the confidence of the same equation. In this numerical example a confidence of approximately 95 % was chosen. Furthermore $\hat{\bar{\boldsymbol{P}}}$ was chosen according to Section 4.4. Also note that $\bar{\psi}_{ref}$ and L_{ref} were chosen so that the upper energy bound as well as the length axis should be one at the fourth data point.

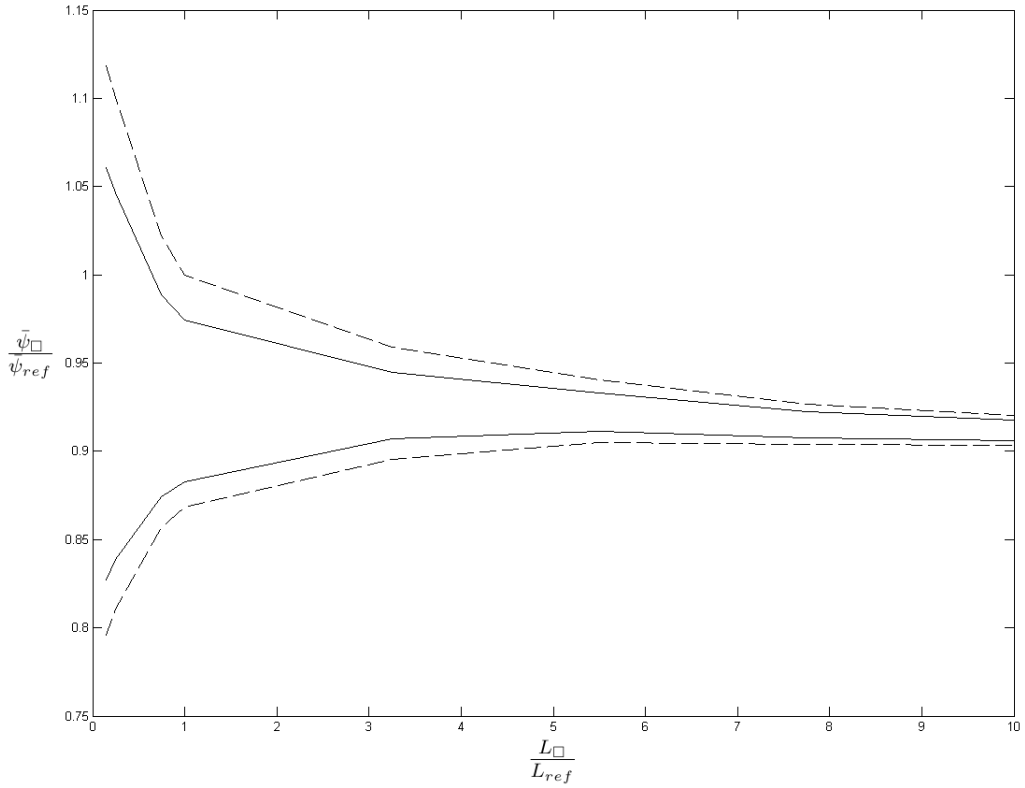

Figure 5.1.1: *The upper and lower bounds of the strain energy as a function of the RVE-size.*

The figure clearly shows that a larger RVE creates tighter bounds on the strain energy. When the size of the RVE approaches zero the bounds obviously diverge to two different values. As a matter of fact, that kind if behavior is expected and it can be shown analytically (although not done here) that the upper bound approaches the Voigt bound and the lower

bound approaches the Reuss bound as the size of the RVE approaches zero.

5.2 Influence of $\tilde{\bar{\boldsymbol{P}}}$ on the lower bound

As been mentioned before, the choice of $\tilde{\bar{\boldsymbol{P}}}$ will affect the lower bound of the strain energy. In order to investigate how good the approximation of section 4.4 really is, two other choices were tested. Furthermore, a totally different approximation of the lower bound was investigated. This is discussed in more detail below together with the results in Figure 5.2.1.

- The upper solid/diamond line of Figure 5.2.1 corresponds to the Voigt bound of the strain energy. It is calculated as follows:

$$\bar{\psi}^V(\bar{\boldsymbol{H}}) = n\psi_{inc}(\bar{\boldsymbol{H}}) + (1-n)\psi_{mat}(\bar{\boldsymbol{H}}) \tag{5.2.1}$$

  where ψ^V is the Voigt bound, n is the theoretical volume fraction, ψ_{inc} is the strain energy in the inclusion material and ψ_{mat} is the strain energy in the matrix material.

- Number (1) shows $\tilde{\bar{\boldsymbol{P}}} : \bar{\boldsymbol{H}} - \mu[\bar{\psi}^{*N}_{\square}\{\tilde{\bar{\boldsymbol{P}}}, \tilde{\omega}_i\}_{i=1}^N]$, i.e equation (3.4.20) without the confidence interval, when $\tilde{\bar{\boldsymbol{P}}}$ is chosen according to Section 4.4, i.e. $\tilde{\bar{\boldsymbol{P}}} = \mu[\bar{\boldsymbol{P}}^N_{\square}\{\bar{\boldsymbol{H}}, \omega_i\}_{i=1}^N]$.

- Number (2) shows $\tilde{\bar{\boldsymbol{P}}} : \bar{\boldsymbol{H}} - \mu[\bar{\psi}^{*N}_{\square}\{\tilde{\bar{\boldsymbol{P}}}, \tilde{\omega}_i\}_{i=1}^N]$ from equation (3.4.20) when $\tilde{\bar{\boldsymbol{P}}} = \mu[\bar{\boldsymbol{P}}^D_{\square}\{\bar{\boldsymbol{H}}, \omega_i\}_{i=1}^N]$.

- Number (3) shows $\tilde{\bar{\boldsymbol{P}}} : \bar{\boldsymbol{H}} - \mu[\bar{\psi}^{*N}_{\square}\{\tilde{\bar{\boldsymbol{P}}}, \tilde{\omega}_i\}_{i=1}^N]$ from equation (3.4.20) when $\tilde{\bar{\boldsymbol{P}}} = \bar{\boldsymbol{P}}^V$ and the Voigt stress $\bar{\boldsymbol{P}}^V$ is defined as:

$$\bar{\boldsymbol{P}}^V(\bar{\boldsymbol{H}}) = n\boldsymbol{P}_{inc}(\bar{\boldsymbol{H}}) + (1-n)\boldsymbol{P}_{mat}(\bar{\boldsymbol{H}}) \tag{5.2.2}$$

  where $\boldsymbol{P}_{inc}$ represents the stress for the inclusion material given $\bar{\boldsymbol{H}}$ and $\boldsymbol{P}_{inc}$ is the corresponding stress for the inclusion material.

- "Approx. LB" represents the approximate choice of $\bar{\psi}^{LB}_{\square}$ used in for example Larsson et al. [7]. It is the sample mean of the strain energy from a Neumann problem; $\mu[\bar{\psi}^N_{\square}\{\bar{\boldsymbol{H}}, \omega_i\}_{i=1}^N]$.

- The lower dashed line in the figure is the approximate[1] Reuss bound of the strain energy, $\bar{\psi}^R$. It can be calculated according to:

$$\bar{\psi}^R = \hat{\bar{\boldsymbol{P}}} : \bar{\boldsymbol{H}} - n\psi^*_{inc}(\hat{\bar{\boldsymbol{P}}}) - (1-n)\psi^*_{mat}(\hat{\bar{\boldsymbol{P}}}) =$$
$$\hat{\bar{\boldsymbol{P}}} : (\bar{\boldsymbol{H}} - n\bar{\boldsymbol{H}}_{inc}(\hat{\bar{\boldsymbol{P}}}) - (1-n)\bar{\boldsymbol{H}}_{mat}(\hat{\bar{\boldsymbol{P}}})) + n\psi_{inc}|_{\hat{\bar{\boldsymbol{P}}}} + (1-n)\psi_{mat}|_{\hat{\bar{\boldsymbol{P}}}} \tag{5.2.3}$$

  In this case $\hat{\bar{\boldsymbol{P}}}$ was chosen to be equal to $\bar{\boldsymbol{P}}^V$. Also note that both the true volume fractions and the theoretical ones were used in the equation above. It appears that the

[1] The formal Reuss bound is obtained from equation (3.4.25). Here we consider the approximation $\bar{\psi}^R(\bar{\boldsymbol{H}}) \approx \bar{\boldsymbol{P}}^V : \bar{\boldsymbol{H}} - E[\bar{\psi}^*(\bar{\boldsymbol{P}}^V)]$ described above.

"real" Reuss bound-curve is somewhat uneven due to the quality of the meshes and the sample size, while the "theoretical" Reuss bound-curve is a straight line since it is mesh independent. The reason why the "real" Reuss-curve is plotted is that it can be seen that (3) converges to a value below the theoretical bound for $L_\square \to 0$. However, it is always above the "real" Reuss curve, see the derivations below.

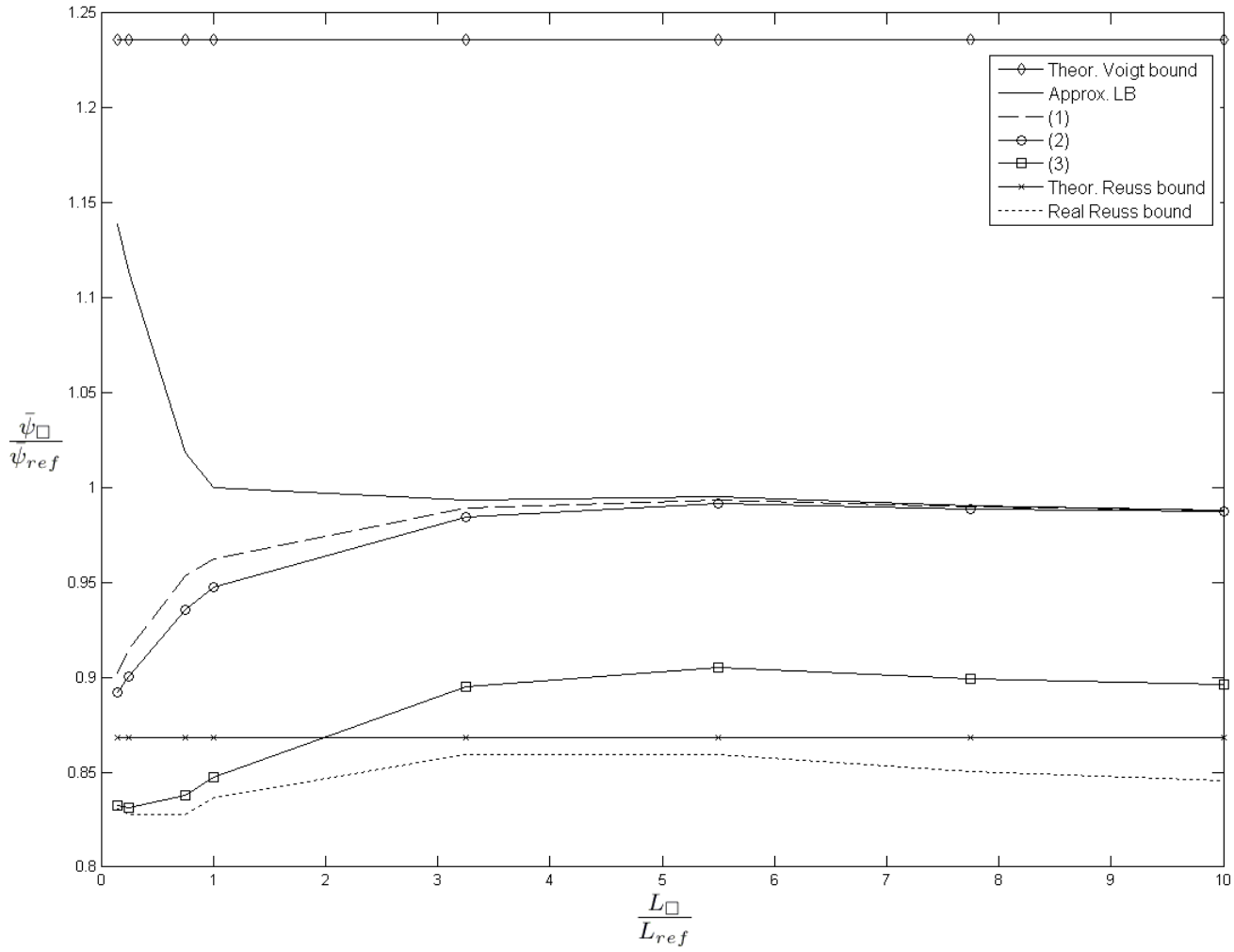

Figure 5.2.1: *The figure shows different approximations of the lower bound. "Approx. LB" corresponds to* $\mu[\bar{\psi}_\square^N\{\bar{\boldsymbol{H}}, \omega_i\}_{i=1}^N]$ *and "(1)-(3)" correspond to the three different approximations tested for* $\hat{\bar{\boldsymbol{P}}}$*. Furthermore the Voigt bound based on theoretical volume fractions and the Reuss bounds based on both theoretical and real volume fractions are shown.*

Some things might be concluded from Figure 5.2.1. First of all, it can be seen that the approximate lower bound approaches the Voigt bound as the size of the RVE approaches zero. This follows directly from equation (3.4.11) if the sample size approaches infinity.

Furthermore, it may be noticed that "Approx. LB" is a relatively good approximation for large RVEs. Besides, it is always larger than (1)-(3). This can also be showed analytically in

the following way with help of equation (3.3.8):

$$\mu[\bar{\psi}_{\square}^{N}\{\bar{\boldsymbol{H}}\}] = \frac{1}{N}\sum_{i=1}^{N}(\max_{\hat{\boldsymbol{P}}_i\in\mathbb{R}^{3x3}}\{\hat{\boldsymbol{P}}_i : \bar{\boldsymbol{H}} - \bar{\psi}_{\square,i}^{*N}\{\hat{\boldsymbol{P}}_i\}\}) \geq$$

$$\max_{\hat{\boldsymbol{P}}\in\mathbb{R}^{3x3}}\{\frac{1}{N}\sum_{i=1}^{N}(\hat{\boldsymbol{P}} : \bar{\boldsymbol{H}} - \bar{\psi}_{\square,i}^{*N}\{\hat{\boldsymbol{P}}\})\} = \max_{\hat{\boldsymbol{P}}\in\mathbb{R}^{3x3}}\{\hat{\boldsymbol{P}} : \bar{\boldsymbol{H}} - \frac{1}{N}\sum_{i=1}^{N}\bar{\psi}_{\square,i}^{*N}\{\hat{\boldsymbol{P}}\}\} =$$

$$\max_{\hat{\boldsymbol{P}}\in\mathbb{R}^{3x3}}\{\hat{\boldsymbol{P}} : \bar{\boldsymbol{H}} - \mu[\bar{\psi}_{\square,i}^{*N}\{\hat{\boldsymbol{P}}\}]\} \geq \hat{\hat{\boldsymbol{P}}} : \bar{\boldsymbol{H}} - \mu[\bar{\psi}_{\square,i}^{*N}\{\hat{\hat{\boldsymbol{P}}}\}] \tag{5.2.4}$$

where $\hat{\hat{\boldsymbol{P}}}$ is an arbitrary choice.

5.3 Stress-strain relations

As been mentioned before, it is possible to construct $\bar{\bar{\psi}}_{\square}$ when $\bar{\psi}_{\square}^{UB}$ and $\bar{\psi}_{\square}^{LB}$ have been calculated. With help of curve fitting it is then possible to obtain $\bar{E}, \bar{\nu}, \bar{h}, \bar{\sigma}_y$ and create $\bar{\psi}_{\square}^{expl}$ as well as a stress-strain relation. But in order to evaluate these results, the RVE with a strain diagram closest to $\bar{\bar{\psi}}_{\square}$, here called $\bar{\psi}_{\square}^{best}$, might be investigated. This has been done for a case with uniaxial strain control and a sample size of 100 RVEs.

The upper diagram of Figure 5.3.1 shows the strain energy curves for all RVEs of the test. The lower diagram is the zoomed in version of the upper one, which makes it easier to see what is meant by the energy curve closest to $\bar{\bar{\psi}}_{\square}$. The solid line represents $\bar{\bar{\psi}}_{\square}$, the dashed lines energy curves for different RVE realizations and the solid line with the square is the curve for that RVE closest to $\bar{\bar{\psi}}_{\square}$.

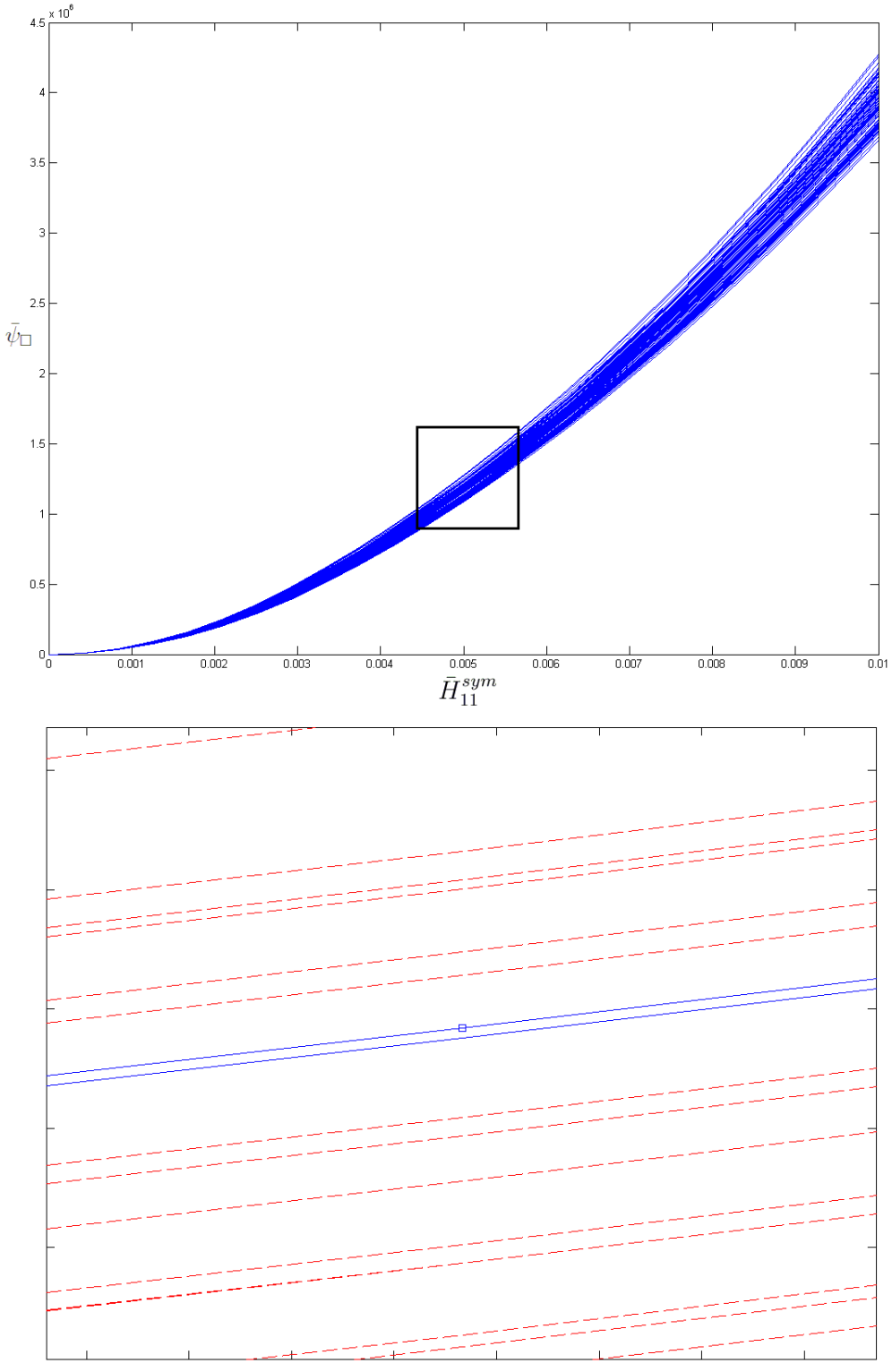

Figure 5.3.1: *The upper diagram shows the strain energy curves, for every RVE, during uniaxial strain loading. When it comes to the lower diagram, the solid line represents* $\bar{\bar{\psi}}_{\square}$*, the dashed lines are the energy curves for different realizations and the solid square line is the "best" RVE.*

It is now possible to compare the "best" RVE realization with $\bar{\bar{\psi}}_{\square}$ and $\bar{\psi}_{\square}^{expl}$. In Figure 5.3.2, $\bar{\psi}_{\square}^{UB}$, $\bar{\psi}_{\square}^{LB}$, $\bar{\bar{\psi}}_{\square}$, $\bar{\psi}_{\square}^{best}$ and $\bar{\psi}_{\square}^{expl}$ are compared. Since the bounds are relatively sharp it might be difficult to identify the individual curves; therefore, the curves are zoomed in two steps.

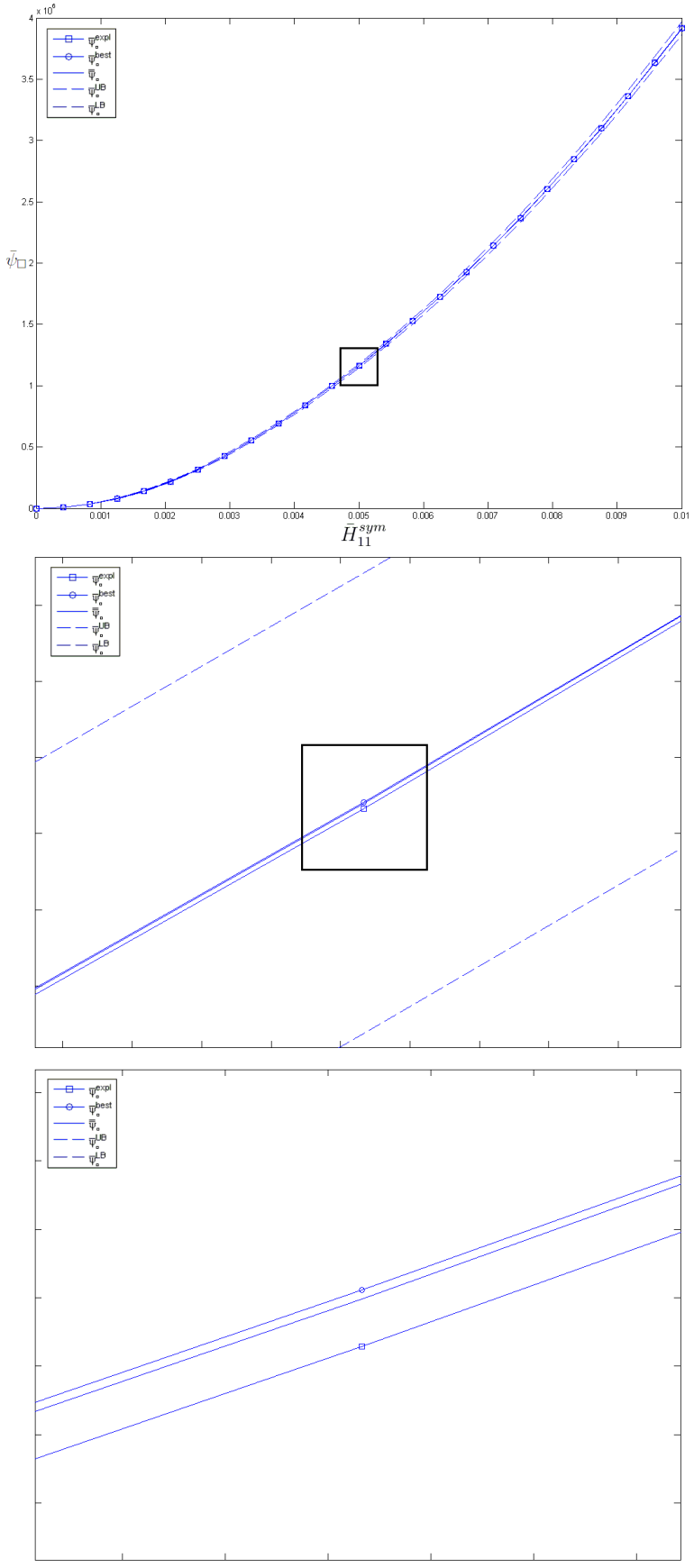

Figure 5.3.2: *Comparison between* $\bar{\psi}_{\square}^{UB}$, $\bar{\psi}_{\square}^{LB}$, $\bar{\bar{\psi}}_{\square}$, $\bar{\psi}_{\square}^{best}$ *and* $\bar{\psi}_{\square}^{expl}$. *The two lower plots are zoomed in versions of the upper plot.*

In order to investigate how close to $\bar{\bar{\psi}}_{\square}$ $\bar{\psi}_{\square}^{expl}$ and $\bar{\psi}_{\square}^{best}$ really are, the error can be plotted as in Figure 5.3.3. Then it is possible to study the error for each strain increment.

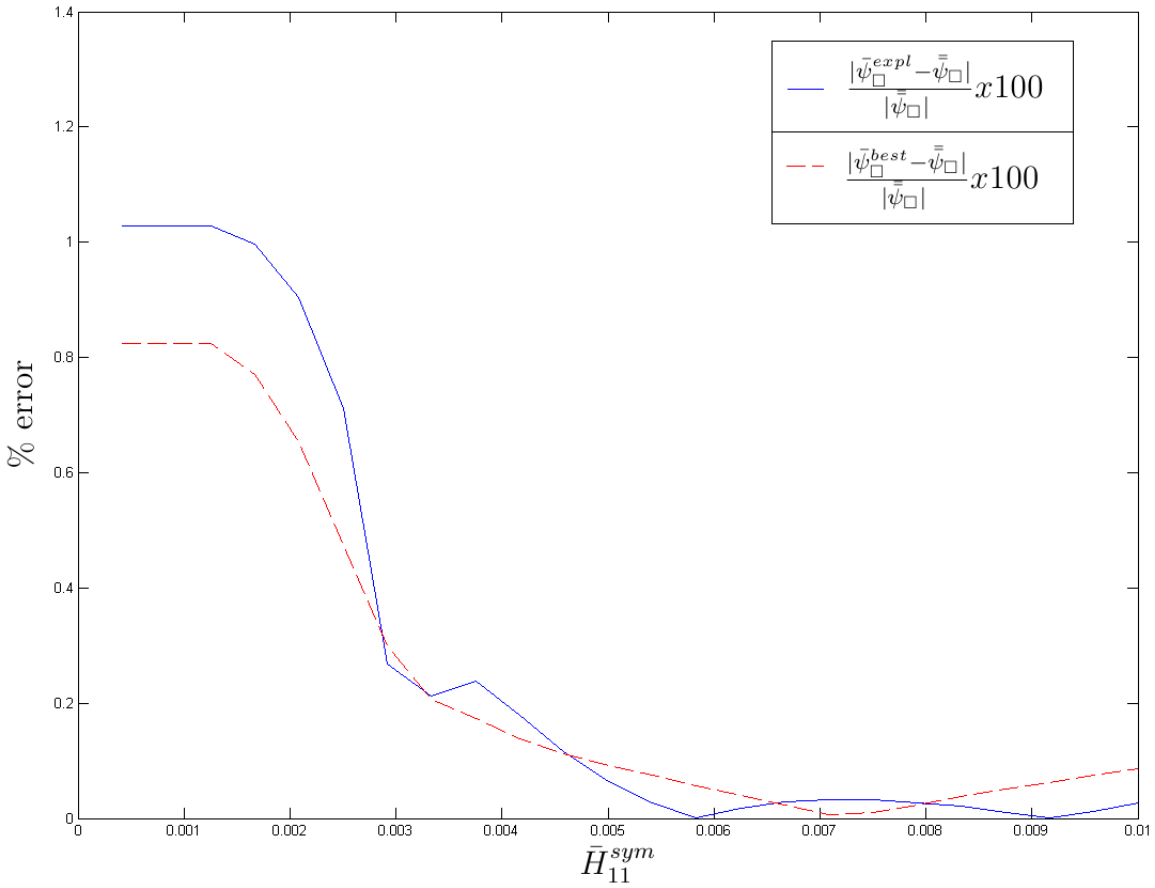

Figure 5.3.3: *The error, defined as in the figure, for each strain increment.*

Finally, it is of course of interest to compare the actual stress-strain relations for the methods of fitted parameters and the one of the "best" RVE. This is shown in Figure 5.3.4. It can clearly be seen that the curves are similar for each stress component, which also infers that the method of fitted constants can be used to produce realistic results.

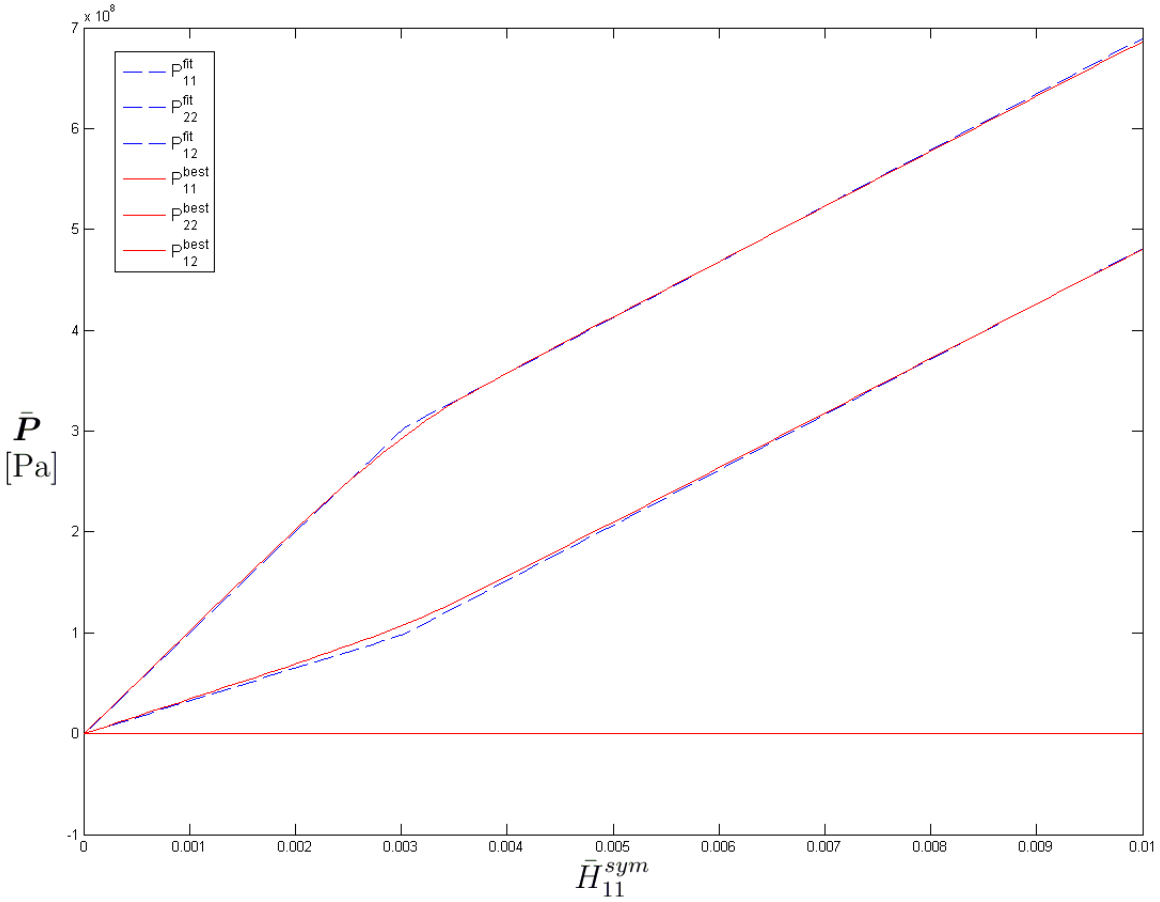

Figure 5.3.4: *The dashed line is constructed with the fitted parameters, while the solid one is the (smooth) stress response from the "best" RVE.*

One last test was also done when the fitted parameters were used in the case of pure shear, which means that $\bar{\gamma}_{12} = 2\bar{\boldsymbol{H}}^{sym}_{12}$ was controlled. The corresponding stress curves were then compared with the same "best" RVE from the previous example. The result is shown in Figure 5.3.5. It can be seen that the normal components of the stresses are all zero or almost zero compared to the magnitude of the shear stresses. The agreement between the "best" RVE and the curve based on fitted parameters is not as accurate as in the case of tensile strain loading but the curves still show good agreement.

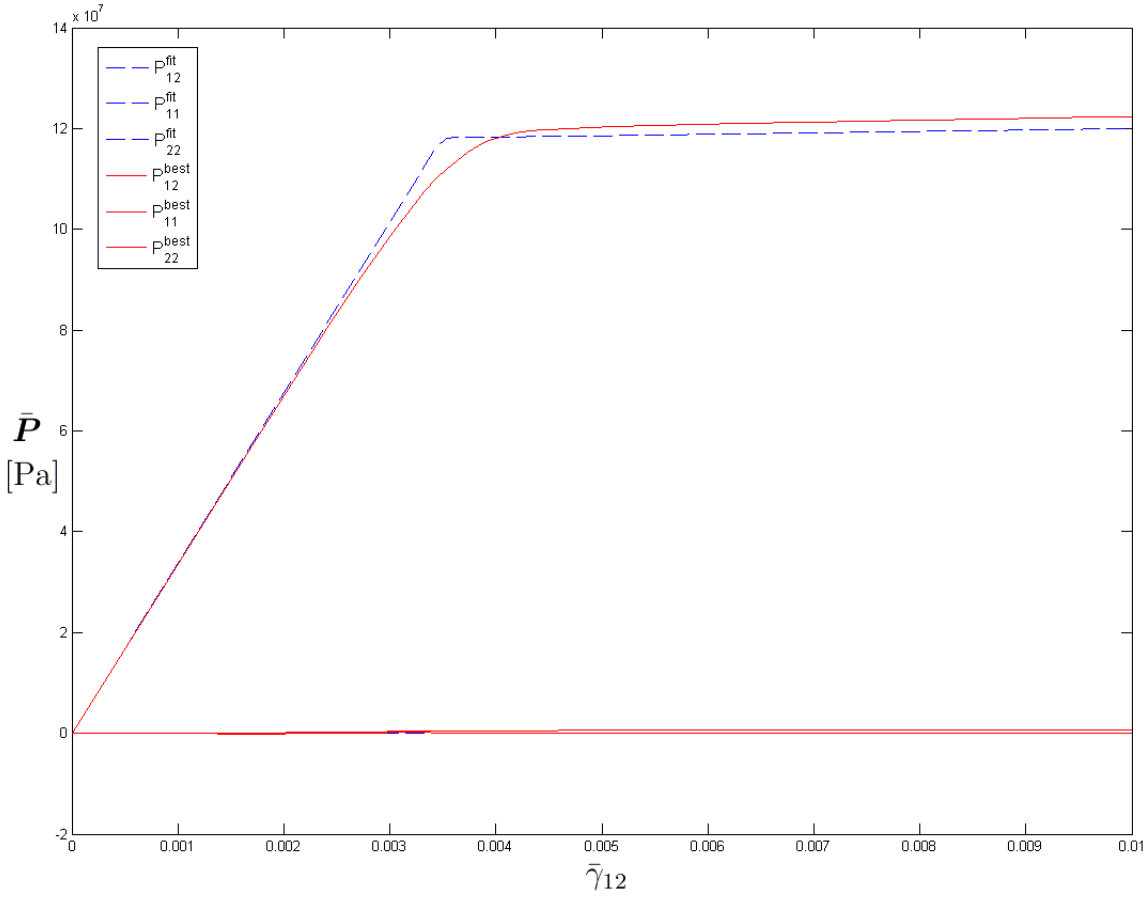

Figure 5.3.5: *The stress curves based on the fitted parameters are compared with the corresponding curves from the "best" RVE in the case of a pure shear strain load.*

6 Conclusions

The purpose of this study was to obtain computable upper and lower bounds on the macroscale strain energy for a two phase composite with circular inclusions and a linear hardening material behavior. From these energy bounds it was desired to construct full macroscopic stress-strain relations. A strategy for constructing the bounds on the macroscopic strain energy as well as a strategy for obtaining the stress-strain relation has been presented. The energy and stress-strain relations based on the method of fitted constants have also been compared to a "best" RVE, i.e. the most representative realization, and shown a reasonable good agreement.

The strategy of obtaining a stress-strain-response with use of fitted constants could in the future be used in engineering practice by considering RVEs based on real material structures and real material properties. The constants could then be used in a material model and implemented in a FE-program.

However, several issues remain to be developed in future works. One important thing of interest would be to calculate $\tilde{\bar{\boldsymbol{P}}}$ according to equation (3.4.21), which produces the sharpest lower bound. $\tilde{\bar{\boldsymbol{P}}}$ could then be compared with the approximate choices presented in this work.

Furthermore, it could be of interest to implement a more advanced material model, involving internal variables, so for example cyclic behavior could be modeled. That should be possible by following the general strategy suggested in this study but requires tracing of the evolution of the subscale deformation with time.

References

[1] T. Asada and N. Ohno. "International Journal of Solids and Structures". In: *Computer Methods in Applied Mechanics and Engineering* 44, Issues 22-23 (2007), pp. 7261–7275.

[2] J. Besson et al. *Non-Linear Mechanics of Materials*. Springer, 2010. ISBN: 978-90-481-3355-0.

[3] I. Doghri and A. Ouaar. "Homogenization of two-phase elasto-plastic composite materials and structures: Study of tangent operators, cyclic plasticity and numerical algorithms". In: *International Journal of Solids and Structures* 40, Issue 7 (2003), pp. 1681–1712.

[4] M. G. D. Geers, V. G. Kouznetsova, and W. A. M. Brekelmans. "Multi-scale computational homogenization: Trends and challenges". In: *Journal of Computational and Applied Mathematics* 234, Issues 7 (2010), pp. 2175–2182.

[5] C. González, J. Segurado, and J. LLorca. "Numerical simulation of elasto-plastic deformation of composites: evolution of stress microfields and implications for homogenization models". In: *Journal of the Mechanics and Physics of Solids* 52, Issue 7 (2004), pp. 1573–1593.

[6] F. Larsson et al. "A computational strategy for obtaining macroscale energy bounds based on homogenization and statistical sampling". In: *Manuscript in preparation* (2011).

[7] F. Larsson et al. "Computational homogenization based on a weak format of micro-periodicity for RVE-problems". In: *Computer Methods in Applied Mechanics and Engineering* 200, Issues 1-4 (2011), pp. 11–26.

[8] C. Miehe, J. Schröder, and J. Schotte. "Computational homogenization analysis in finite plasticity Simulation of texture development in polycrystalline materials". In: *Computer Methods in Applied Mechanics and Engineering* 171, Issues 3-4, (1999), pp. 387–418.

[9] F. Nilenius et al. "Modellering och simulering av fukt- och kloridjonstransport i betongens mikrostruktur". In: *Bygg och Teknik* 102, Issue 7 (2010), pp. 50–54.

[10] M. Ostoja-Starzewski. *Microstructural Randomness and Scaling in Mechanics of Materials*. Chapman and Hall/CRC, 2007. ISBN: 9781584884170.

[11] S. Quilici and G. Cailletaud. "FE simulation of macro-, meso- and micro-scales in polycrystalline plasticity". In: *Computational Materials Science* 16, Issues 1-4, (1999), pp. 383–390.

[12] F. Roters et al. "Overview of constitutive laws, kinematics, homogenization and multiscale methods in crystal plasticity finite-element modeling: Theory, experiments, applications". In: *Acta Materialia* 58, Issue 4 (2010), pp. 1152–1211.

[13] K. Terada et al. "Simulation of the multi-scale convergence in computational homogenization approaches". In: *International Journal of Solids and Structures* 37, Issue 16 (2000), pp. 2285–2311.

[14] C. Wellmann, C. Lillie, and P. Wriggers. "Homogenization of granular material modeled by a three-dimensional discrete element method". In: *Computers and Geotechnics* 35, Issue 3 (2008), pp. 394–405.